Cyclin A2 Induces Human Adult Cardiomyocyte Cytokinesis and Elicits Cardiomyocyte Reprogramming and Dedifferentiation

Esmaa Bouhamida[1], Sangeetha Vadakke-Madathil[1#], Prabhu Mathiyalagan[2#], Amaresh K. Ranjan[1,3#], Amir Khan[1], Cherrie D. Sherman[1], Paul E Miller[4], Andre Ghetti[4], Najah Abi-Gerges[4] and Hina W. Chaudhry[1*]

[1] Icahn School of Medicine at Mount Sinai, New York, NY 10029, USA
[2] Benthos Prime Central, TX, USA
[3] Pharmazz Inc., Willowbrook, IL, USA, 60527
[4] AnaBios Corporation, San Diego, CA 92109, USA
[#] Contributed equally

* Correspondence to

Hina W. Chaudhry, M.D., Department of Cardiology, Cardiovascular Regenerative Medicine, Mount Sinai School of Medicine, One Gustave L. Levy Place, Box 1030, New York, NY 10029, Phone: 212-241-4104, Fax: 212-241-5510. hina.chaudhry@mssm.edu.

Abstract

Cyclin A2 (CCNA2), a master cell cycle regulator, is silenced in postnatal mammalian cardiomyocytes. We have previously demonstrated its ability to promote cardiac repair in small and large animals when delivered to the heart via a viral vector. However, the effect of CCNA2 gene delivery on cytokinesis in isolated cardiomyocytes from adult human hearts has not been explored. We designed a human gene therapy vector featuring a replication-deficient adenovirus encoding human CCNA2 driven by the cardiac Troponin T promoter to enable the expression of CCNA2 in freshly isolated human cardiomyocytes. Time-lapse live imaging of adult human primary cardiomyocytes from a 21-year-old male, a 41-year-old female, and a 55-year-old male demonstrated the induction of complete cytokinesis in human adult cardiomyocytes with preservation of sarcomere integrity in the resulting daughter cells with active calcium mobilization in redifferentiated cardiomyocytes. To elucidate the transcriptional mechanisms underlying this response, we conducted single-nucleus transcriptomics analysis of hearts isolated from adult transgenic mice that constitutively express CCNA2 in cardiomyocytes (CCNA2-Tg) and non-transgenic mice (nTg). This revealed a cardiomyocyte subpopulation enriched with cytokinesis, proliferative, and reprogramming genes in hearts obtained from CCNA2-Tg mice as compared to nTg mice. Ultra-deep bulk RNA sequencing of human adult and fetal hearts identified key reprogramming genes relevant to understanding the mechanisms of CCNA2-induced effects observed in our experimental models. These findings provide a promising path for the clinical development of CCNA2-based cardiac regenerative therapy.

Graphical Abstract

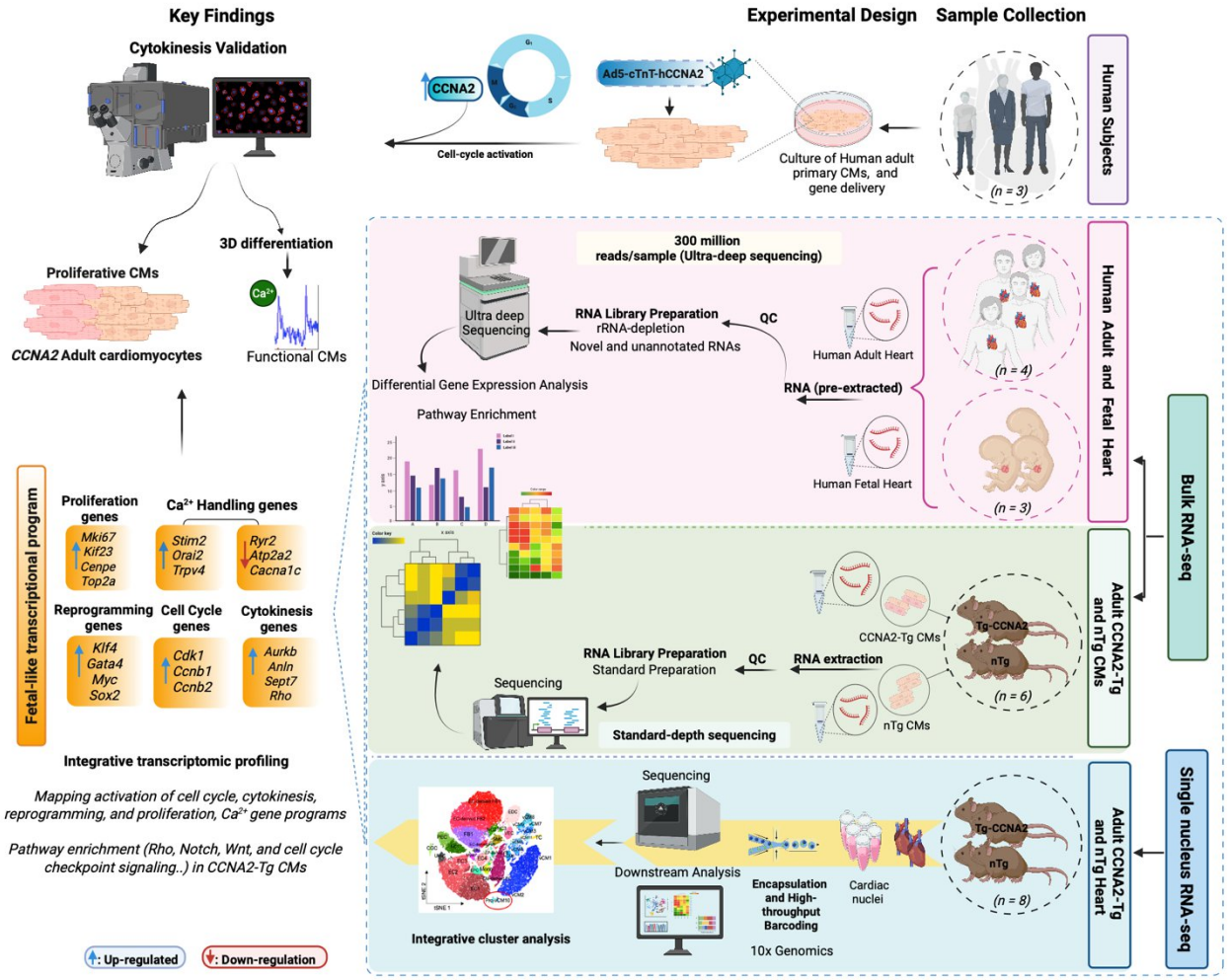

CCNA2 Induces Cytokinesis and Drives Proliferation and Reprogramming of Adult Cardiomyocytes: An Integrative Transcriptomic Analysis across Human and Mouse Models.

Introduction

The limited proliferative capacity of adult human cardiomyocytes remains a major barrier to effective cardiac regeneration following injury, contributing to the significant morbidity and mortality associated with heart disease [1]. Scar formation via fibrosis is, therefore, the primary response to cardiac injury. Multitudes of molecular and cellular approaches have been investigated over the past 20 years aimed at regenerating the myocardium in various states of heart disease [2-4]. The use of stem/progenitor cell therapies for myocardial regeneration has demonstrated limited efficacy in clinical trials, with no conclusive evidence of actual cardiomyocyte differentiation arising from the cell types used previously in these trials. Human embryonic stem (ES) cells and induced pluripotent (iPS) cells have been evaluated in non-human primate models of heart disease with the demonstrated ability of these cell types to differentiate, at the very least, to immature cardiomyocytes with the hope that they would undergo maturation *in vivo.* However, it remains to be seen whether these approaches may be translated for human therapy [3,5]. Aside from the differentiation and generation of new cardiomyocytes, some technical concerns still need to be addressed, such as the propensity for arrhythmias noted in primate hearts treated with ES-derived and iPS-derived cardiomyocytes [5,6].

There has been evidence of low-level cardiomyocyte turnover in the healthy human heart, but it is very limited, and this ability declines with age [7,8]. Thus, cardiac regeneration in response to injury such as myocardial infarction (MI) remains a clinical challenge. Evolution may not have favored adult mammals in this regard, but certain members of metazoan species are capable of heart regeneration, and these examples may perhaps serve to enlighten us. Urodele amphibians, such as the newt, retain a remarkable capacity to replace lost anatomical tissues through epimorphic regeneration [9]. This process relies on the local plasticity of differentiated cells near the region of injury and involves reentry to the cell cycle with loss of differentiated characteristics to generate a 'local progenitor cell' of restricted potentiality [9]. The adult zebrafish heart can regenerate up to 20% of its volume via a mechanism largely dependent on the proliferation of cardiomyocytes adjacent to the area of injury [10,11]. However, zebrafish harboring a temperature-sensitive mutation in *mps1*, a gene encoding a mitotic checkpoint kinase [10], cannot regenerate the heart, and scarring and fibrosis are noted in the excised areas in a manner similar to the response of the human myocardium after injury [10,12]. In summary, the loss of a single gene can avert cardiomyocyte mitosis and mitigate the normal regenerative process, thus permitting fibrosis to proceed unimpeded.

Previously, we have reported that CCNA2 is a 'master regulator' of the cardiomyocyte cell cycle [13]. Unlike other cyclins, cyclin A2 complexes with its cyclin-dependent kinase partners to regulate both key transitions of the cell cycle: G1-S and G2-M [14-16], and is silenced shortly after birth in mammalian cardiomyocytes [1,17,18]. Subsequently, we have also shown that *Ccna2* mediates cardiac repair by inducing cardiomyocyte mitoses after MI in two small animal models of MI [19-21]. As molecular mechanisms may be widely divergent across species, we performed a therapeutic efficacy study of CCNA2-mediated cardiac repair in a porcine model of MI as it closely mimics human anatomy and physiology [22]. Therapeutic delivery of *CCNA2* one week after MI in the porcine heart induced cardiomyocyte cell cycle activation *in vivo* with marked enhancement of

cardiac function as noted with multimodality imaging, including magnetic resonance imaging. The experimental pigs also exhibited significantly decreased fibrosis, lack of cardiomyocyte hypertrophy, and a 55% increase in cardiomyocyte cell numbers in the peri-infarct zones. Using the same viral vector encoding CCNA2 that was delivered *in vivo*, cultured porcine adult cardiomyocytes were induced to undergo cytokinesis with preservation of sarcomere structure and captured via live imaging [22].

For the purposes of clinical translation, we designed the next-generation gene therapy vector using a cardiomyocyte-specific promoter, cardiac Troponin T (cTnT), driving human CCNA2 expression. We then sought to determine whether this cTnT-CCNA2 vector would induce human adult cardiomyocytes to undergo cytokinesis. We employed a multiparametric approach combining live-cell imaging with high-resolution transcriptomics to uncover mechanistic insights underlying CCNA2-driven cytokinesis in adult cardiomyocytes. Live imaging microscopy enabled dynamic tracking of sarcomere integrity and cellular architecture during cytokinesis in adult human cardiomyocytes. To dissect the transcriptional programs and signaling pathways associated with *CCNA2* expression, we leveraged three complementary RNA sequencing datasets: (i) bulk RNA-sequencing of CCNA2-Tg and nTg cardiomyocytes, (ii) ultra-deep bulk RNA-sequencing of adult and fetal human hearts, and (iii) single-nucleus RNA sequencing (snRNA-seq, 10x Genomics).

This integrative approach defined the molecular framework by which CCNA2 reactivates cell cycle networks, promotes cytokinesis, and induces a regenerative transcriptional state in postnatal cardiomyocytes, offering insights for future cardiac regenerative therapies.

Results

cTnT-CCNA2 adenovirus vector designed for therapeutic use induces expression of CCNA2 in cultured adult human cardiomyocytes

First, we designed a therapeutic grade human CCNA2 adenovirus vector to selectively express human cyclin A2 (CCNA2) in cardiomyocytes by cloning human cDNA (NCBI Reference Sequence: NM_001237.4; 374-1672 bp) downstream to the cTnT promoter **(Figure 1A)**. The cultured adult human cardiomyocytes were transduced with cTnT-hCCNA2 (test) versus cTnT-eGFP (control) adenoviruses with a multiplicity of infection (MOI) of 100 each for assessing the induced expression of CCNA2. We observed significantly increased expression of CCNA2 in the cultured adult human cardiomyocytes transduced with the test compared to the control adenovirus (**Figure 1B**). We utilized cTnT-H2B-GFP to confirm that the nuclei of the daughter cells belonged to cardiomyocytes.

Adenoviral vector-mediated expression of CCNA2 induces cytokinesis in cultured adult human cardiomyocytes

To assess the effect of induced CCNA2 expression on cell division in adult human cardiomyocytes, we cultured adult human cardiomyocytes and studied cytokinesis *in vitro* by using live cell epifluorescence time-lapse microscopy. The adult human cardiomyocytes were plated at equal densities and transduced with cTnT-hCCNA2, cTnT-eGFP and/or cTnT-H2B-GFP and CMV-α-act-mCherry adenoviruses (test) or with cTnT-eGFP and/or cTnT-H2B-GFP and CMV-α-act-mCherry adenoviruses (control). cTnT-eGFP and/or cTnT-H2B-GFP adenovirus was transduced in both groups to confirm the initial tracking of cardiomyocytes (green) during live cell epifluorescence microscopy. For live visualization of sarcomeric structure in cardiomyocytes, cells from both groups were co-transduced with adenovirus containing α-act-mCherry, which we had constructed to allow for proper folding of the virally delivered α-actinin into the live cardiomyocyte sarcomere (CMV-α-act-mCherry) and was successfully used in cultured adult porcine cardiomyocytes [22]. This strategy enabled us to confirm cardiomyocyte identity by assessing the expression of eGFP before and after cytokinesis and tracking sarcomere dynamics during live cell imaging. This approach provides a significant advantage over antibody-based identification, which is susceptible to artifacts and restricted to a single time point after cell fixation. We observed co-expression of eGFP (green) and α-actinin (red) in cultured adult cardiomyocytes **(Figure 1C** and **1H**; first panel). We performed time-lapse microscopic imaging of live cells to capture cardiomyocyte cytokinesis **(Figure 1C**, **1F**, and **1H**; still images from **movie S1)**. The cytokinetic index of adult human cardiomyocytes was calculated by counting the cytokinetic events observed in 42 regions of interest (ROIs) **(Source Data Figure 1I)**. The cytokinetic index was significantly higher in the test samples with cTnT-CCNA2 adenovirus transduction compared to control samples in the 41- and 55-year-olds **(Figure 1I)**. In contrast, no significant change in the cytokinetic events between test and control samples was observed in the 21-year-old patient's cardiomyocytes **(Figure 1I)**. Most remarkably, sarcomere structure was preserved in the daughter cells after cytokinesis **(Figure 1D** and **Figure 1G**; upon magnification of a daughter cell, the presence of sarcomeric structure is easily noted). The daughter cells were further identified with the expression of H2B-GFP (as they were originally also transduced with cTnT-eGFP and/or H2B-GFP) and noted to be mononuclear after they had been fixed and stained with DAPI **(Figure 1E** and **1H)**. Clusters of other cardiomyocytes with expression of eGFP could be seen adjacent to the daughter cells **(Figure 1E)**.

Next, we assessed the functional differentiation of cardiomyocytes by measuring the Ca^{2+} transients in CCNA2-expressing cardiomyocytes using live-cell calcium imaging under pacing conditions (0.5 Hz and 1 Hz; **Figure 2A**). Cardiomyocytes transduced with Ad5-cTnT-hCCNA2 exhibited active Ca^{2+} transients **(Figure 2B)**. These findings demonstrate that CCNA2 drives cytokinesis while preserving sarcomere integrity and calcium mobilization in adult human cardiomyocytes, suggesting functional differentiation.

CCNA2 reprogramming induces fetal gene signatures for calcium handling and sarcomere dynamics

To quantify the developmental and reprogramming landscape, we performed ultra-deep bulk RNA-sequencing of fetal (n=3) and adult (n=4) human hearts. This approach allowed us to compare the molecular signatures of CCNA2-induced cardiomyocyte reprogramming with naturally occurring fetal-like states. Our ultra-deep sequencing approach enhanced our ability to

188 detect low-abundance transcripts, improve quantification accuracy, and provide a more
189 comprehensive transcriptomic profile. This comparison contextualizes how CCNA2 expression
190 modulates gene networks associated with dedifferentiation, proliferation, and calcium handling,
191 highlighting its role in cardiac plasticity and regeneration. Notably, there were overlapping
192 differentially expressed genes (DEGs) between adult CCNA2-Tg mouse cardiomyocytes and
193 fetal human hearts with downregulated genes in both that were associated with cardiomyocyte
194 maturation **(Figure 2C and 2D)**. Furthermore, we found that calcium handling and contractility-
195 related genes, as well as sarcomere assembly genes such as *RYR2, ATP2A2, SLC8A1, CALM1,*
196 *CALM2, NEB, TTN*, and *TNNC1* were differentially upregulated in adult human hearts compared
197 to fetal human hearts **(Figure 2E)**.
198
199 Additionally, we performed bulk RNA-sequencing of mouse cardiomyocytes with constitutive
200 CCNA2 expression in cardiomyocytes (CCNA-Tg mice) compared to non-Tg mice (n=6 in total).
201 Key calcium handling genes, including *Ryr2, Atp2a2, Slc8a1,* and sarcomere assembly genes as
202 well as *Neb, Ttn,* and *Tnnc1,* were significantly downregulated in CCNA2-Tg cardiomyocytes. In
203 contrast, genes involved in intracellular calcium release and store-operated calcium entry, such
204 as *Itpr1, Orai2,* and *Stim2*, were upregulated in CCNA2-Tg mouse hearts, further aligning with
205 the fetal gene expression profile **(Figure 2F and S1)**. This suggests that *CCNA2* may regulate
206 sarcomere assembly genes during cell division **(Figure S1)**, thereby facilitating cardiomyocyte
207 proliferation [23]. Furthermore, *CCNA2* appears to influence calcium mobilization post-cytokinesis,
208 suggesting a broader role beyond cell cycle regulation, potentially impacting cardiomyocyte
209 maturation and function.
210
211 Live-cell imaging of CCNA2-overexpression in adult human cardiomyocytes undergoing
212 cytokinesis revealed that daughter cells retain sarcomeric integrity post-division. Despite RNA-
213 sequencing data showing a significant downregulation of thin filament genes (*Neb, Tnn, Tnnc1*),
214 structural sarcomere genes such as *Tnnt2* and *Actn2* remained stable **(Figure S1)**, suggesting
215 that sarcomere remodeling may occur transiently to accommodate cell division without leading to
216 complete dedifferentiation. Interestingly, transcriptomic profiling revealed upregulation of *ZEB1*
217 in both fetal hearts and CCNA2-Tg mouse hearts, suggesting a conserved role in cardiomyocyte
218 plasticity **(Figure S1)**. *SNAI1,* a gene implicated in epithelial to mesenchymal transition with roles
219 in cancer development and progression, was not consistently upregulated. However, *ZEB1*'s
220 expression aligns with transient mesenchymal activation, which has been implicated in neonatal
221 heart regeneration [24].
222

223 Single-nucleus transcriptomic profiling reveals CCNA2-driven reprogramming in 224 selective cardiomyocytes, supported by integrative bulk RNA-seq analysis

225
226 To investigate CCNA2-induced cardiomyocyte cytokinesis in an unbiased manner, we performed
227 snRNA-seq on hearts isolated from control non-transgenic (nTg) and *CCNA2* constitutively
228 expressing transgenic (CCNA2-Tg) adult mice (n=8 in total). Both male and female mice aged 8-
229 12 weeks were included. This approach enabled the identification of differentially expressed
230 genes across cardiac clusters in both nTg and CCNA2-Tg mice in the context of CCNA2
231 expression. **(Figure 3A**, **3B**, and **Figure S1)**. Notably, snRNA-seq also captured

underrepresented cell types often lost during enzymatic digestion for single cell RNA-seq, providing a comprehensive view of cardiac cellular heterogeneity [23,25].

t-distributed Stochastic Neighbor Embedding (t-SNE) of combined nuclei profiles from both nTg and CCNA2-Tg mouse hearts revealed 16 major cardiac cell populations, including cardiomyocytes, endothelial cells, fibroblasts, cardiac, immune cells, and neuronal cells, distributed across 35 subclusters **(Figure 3C-E)**. Cell type clusters were annotated based on expression of canonical marker genes and validated through differential expression analysis and comparison with a publicly available reference dataset (iRhythmics FairdomHub) [26,27]. **(Figure 3F, 3G)**.

We identified several common clusters between nTg and CCNA2-Tg mice **(Figure 3E**, **Figure S3)**, with differential distribution across conditions **(Figure 3H and 3I)**. Cardiomyocyte populations were identified by the classical marker genes (*Myh7*, *Actn2,* and *Tnnc1*) in both nTg and CCNA2-Tg hearts. Cardiomyocytes that express an enhanced level of contractility genes, including the *Ryr2*, are annotated as mature cardiomyocytes [27].

SnRNA-seq identified 11 subclusters of the ventricular cardiomyocyte (vCM) population common to both nTg and CCNA2-Tg hearts, with distinct differences in the proportion of nuclei across subclusters. Notably, the vCM1 and vCM5 were more prevalent in nTg hearts, whereas the vCM2, vCM3, vCM4, vCM6, vCM7, vCM8, vCM9, pro-vCM10, and the vCM11 were more abundant in CCNA2-Tg hearts **(Figure 3J)**.

Subclusters vCM1, vCM2, vCM4, vCM5, and vCM11 expressed cardiomyocyte maturation-related genes, particularly sarcomere development genes, calcium (Ca^{2+}) handling, and cardiac contractility genes (*Ttn*, *Pln, Ryr2*, and *Pkp2, Kcnd2*, and *Tnni3k),* regulating cardiomyogenesis and function [28]. Notably, vCM5 also expressed non-cardiac lineage markers such as *Ebf2*, implicated in brown adipocyte differentiation [29], and *Lsamp*, which guides neuronal connections [30]. In contrast, vCM3 and vCM7 showed increased expression of ATP synthase genes (*Atp5b* and *Atp5g3),* while vCM4 and vCM8 co-expressed the endothelial-associated gene vCM9 was uniquely marked by *Igfbp3*, consistent with a mid-differentiation state.

Moreover, the transcriptomic profile of the Pro-vCM10 displayed a robust cell cycle signature with high expression of early-phase proliferative genes (*Top2a, Cdc20, Cdk2d, Cdk1, Prc1 Bub1, Mki67*, and *Kif23)*, and mitotic-cytokinesis drivers (*Stmn1*) [31], alongside adhesion complex assembly and immune markers (*Cd44, and C1qa*) [32]. This transcriptional profile indicates an actively cycling, dedifferentiated cardiomyocyte population poised for regeneration. Remarkably, the proportion of Pro-vCM10 was significantly higher in CCNA2-Tg mouse hearts compared to nTg mouse hearts **(Figure 3J)**.

CCNA2 was expressed in cardiomyocytes, predominantly within the proliferative cluster identified in CCNA2-Tg hearts, which also expressed key cell cycle regulators **(Figure 4A** and **4B)**. This expression pattern remained consistent across the combined transcriptomic profiles of all subclusters **(Figure S4)**. The pro-vCM subcluster in CCNA2-Tg mice co-expressed proliferative

markers (*Mki67* and *Kif23*) and exhibited reduced *Ryr2*, consistent with a less mature phenotype **(Figure 5A** and **5B)**. Compared to nTg cardiomyocytes, where *Ryr2* expression was higher, CCNA2-Tg cardiomyocytes expressed a transcriptional signature consistent with a dedifferentiated state that may facilitate cell cycle re-entry and regeneration [33].

Bulk RNA-sequencing further supported this profile, revealing coordinated downregulation of sarcomere, contractility genes, and upregulation of proliferative programs in CCNA2-Tg cardiomyocytes (**Figure S5A** and **S5B**), aligning with a dedifferentiated state, which facilitates cell cycle re-entry and cytokinesis. This transcriptional 'immaturity' may enable the proliferative potential necessary for myocardial regeneration.

To further examine CCNA2-induced cytokinesis events, we investigated whether distinct cardiomyocyte subclusters expressed genes associated with cytokinesis and/or reprogramming in CCNA2-Tg mice. Intriguingly, the pro-vCM population demonstrated upregulation of core cytokinesis regulators such as *Aurkb, Anln, Sept7,* and *Rho,* among others, with *Rho* and *Aurka* significantly elevated in CCNA2-Tg compared to nTg mice **(Figure 5C)**. This pro-vCM subcluster also showed increased expression of reprogramming genes, including *Pou5f1, Klf4, Gata4, Myc, Sox2,* and *Tbx5*, with *Pou5f1* and *Tbx5* notably increased in CCNA2-Tg hearts compared to nTg hearts **(Figure 5D)**. These findings were consistent with bulk RNA-sequencing analysis, which revealed increased expression of cytokinesis- and reprogramming-associated genes in CCNA2-Tg cardiomyocytes compared to nTg cardiomyocytes **(Figure S5C** and **S5D)**.

Pathway enrichment analysis of CCNA2-Tg cardiomyocytes shows significant activation of cell cycle, cytokinesis, and mitotic regulation pathways compared to nTg controls. Notably, Rho GTPase signaling, spindle checkpoint regulation, and cytokinesis pathways were highly enriched **(Figure 5E)**, indicating increased proliferation and cytoskeletal remodeling in CCNA2-Tg hearts. In contrast, nTg cardiomyocytes showed enrichment in extracellular matrix organization, collagen biosynthesis, and muscle contraction pathways, reflecting a more differentiated state. These findings indicate that CCNA2 enhances proliferation and cellular plasticity, promoting a regenerative phenotype in cardiomyocytes.

Our bulk RNA-sequencing data from mouse nTg and CCNA2-Tg cardiomyocytes yielded comparable findings. We observed upregulation of *Ccnb1* and *Ccnb2* in CCNA2-Tg cardiomyocytes compared to nTg cardiomyocytes, along with slight increases in the expression of *Cdk1* in CCNA2-Tg cardiomyocytes **(Figure 5F)**. *Cdk1* is the sole essential cyclin-dependent kinase (*CDK*), when complexed to Cyclin A2 promotes entry into mitosis, whereas Cyclin A2/Cdk2 is critical for the G1/S transition [13,34,35]. Key cytokinesis and proliferation genes, including *Aurka, Aurkb, Anln, Mki67,* and *Kif23,* were upregulated in CCNA2-Tg cardiomyocytes, reinforcing the role of CCNA2 in cell cycle reactivation **(Figure 5F)**. Adult human hearts exhibited downregulation of proliferative and cytokinesis-related genes **(Figure 5G, 5H)**, whereas CCNA2-Tg cardiomyocytes retained a transcriptional profile favoring cell cycle progression and cytokinesis.

Differential expression analysis further revealed that adult human hearts exhibit a greater number of downregulated genes compared to the fetal heart (**Figure 5I)**, consistent with widespread

transcriptional silencing during cardiomyocyte maturation. In contrast, CCNA2-Tg cardiomyocytes displayed a higher number of upregulated genes relative to nTg controls **(Figure S5E)**, indicating broad transcriptional reactivation. This inverse pattern supports the role of *CCNA2* in restoring a fetal gene expression landscape.

Pathway enrichment analysis of these differentially expressed genes confirmed upregulation of metabolism, Ca^{2+} mobilization, and ion homeostasis pathways in adult human heart, and downregulation of pathways linked to mitotic progression and developmental gene programs **(Figure 5I)**. These findings support the hypothesis that CCNA2 reactivates a fetal-like transcriptional program in adult cardiomyocytes, promoting cell cycle re-entry without complete dedifferentiation.

Furthermore, pathway enrichment analysis revealed activation of key signaling pathways associated with cardiomyocyte plasticity, proliferation, and reprogramming in CCNA2-Tg cardiomyocytes. Specifically, the NOTCH signaling pathway and its downstream effectors (HES/HEY) were upregulated, reinforcing CCNA2's role in progenitor-like gene activation and cardiac reprogramming. Additionally, developmental pathways such as TGF-beta regulation and Wnt interactions suggest a shift toward a more plastic, regenerative state. Increased signaling through MAPK, PDGF, and Jak-STAT pathways further supports enhanced proliferation and cytoskeletal remodeling. Furthermore, upregulation of focal adhesion, integrin interactions, and actin cytoskeleton regulation pathways indicate structural adaptations that facilitate cardiomyocyte dedifferentiation and division. Conversely, mitochondrial metabolism and oxidative phosphorylation, hallmarks of mature cardiomyocyte function, were significantly downregulated, aligning with a metabolic reversion to a fetal-like, proliferative phenotype in CCNA2-Tg cardiomyocytes. **(Figure S5F, S5G)**. Moreover, adult CCNA2-Tg cardiomyocytes exhibit a greater number of upregulated genes compared to nTg cardiomyocytes in mice **(Figure S5E)**.

In summary, our data highlight roles for *CCNA2* to enhance reprogramming and dedifferentiation, which ultimately elicits cardiomyocyte cytokinesis. These results provide a compelling pathway forward for the clinical development of cardiac regenerative therapy based on the manipulation of CCNA2 expression in cardiomyocytes.

Discussion

Epimorphic regeneration is a conserved mechanism across evolutionary biology, permitting organ-specific tissue regeneration in a variety of metazoan phylogeny, including early postnatal mammals [36]. In fact, in human neonates, the ventricular myocardium responds to the pressure overload of congenital aortic stenosis through hyperplastic growth, yet the degenerative, calcific aortic stenosis of older patients elicits hypertrophic growth of the myocardium [37-39]. These clinical observations imply that the cell cycle repertoire of human neonatal cardiomyocytes is also intact, as cardiac growth is able to occur in a similar fashion to the embryonic heart. Moreover, the adult human heart is also capable of a very low rate of turnover [8], with diminishing rates of turnover past childhood and adolescence, with cardiomyocyte cytokinesis markers not found past age 20 [7].

362
363 Strategies to induce cardiomyocyte cytokinesis in adult human hearts are of critical need in order
364 to face the growing public health crisis of congestive heart failure. To our knowledge, most cell
365 therapy clinical trials in heart disease have provided inconsistent evidence of improvements in
366 left ventricular ejection fraction, with a lack of evidence that the cell types utilized actually
367 differentiate into functional cardiomyocytes. To this end, we previously explored the effects of cell
368 cycle manipulation in small and large animal models and successfully induced cardiomyocyte
369 proliferation *in vivo* with significant enhancement of cardiac function in animal models [19,22]. In any
370 translational plan to use cell cycle regulators for clinical use, two angles must be considered.
371 Firstly, the wrong cell cycle regulators can induce cellular apoptosis [40-43] or be ineffective if the
372 G2/M checkpoint is not navigated [13,22,44]. Secondly, precautions must be taken to prevent the
373 expression of cell cycle activators in extra cardiac tissues due to the potential for oncogenic
374 transformation [45]. This safety concern prompted us to explore methods of tissue-specific
375 activation of cyclin A2. One such method was to design a next-generation viral vector in which
376 a cardiomyocyte-specific promoter, cardiac Troponin T, drives the expression of human cyclin A2
377 (cTnT-hCCNA2). Human cardiomyocytes isolated from 21-, 41- and 55-year-olds who had died
378 of noncardiac causes were cultured utilizing adult mammalian cardiomyocyte culture methods
379 developed by our laboratory [22] and transduced with cTnT-hCCNA2. Cardiomyocytes from the 41-
380 and 55-year-olds in the experimental wells underwent complete cytokinesis at a significantly
381 higher frequency than the cardiomyocytes in the control wells. Based on our previous studies of
382 rodent cardiomyocytes, we attribute the low rate of cytokinetic events we observed in the control
383 wells to the reactivation of endogenous *CCNA2* with the prolonged culture of cardiomyocytes.
384 This is a phenomenon we have previously observed and quantified in rodent cardiomyocytes,
385 and likely not correlated with the low turnover seen in human hearts as measured by 14C dating
386 [46] as cytokinesis markers were not noted at all in human hearts over the age 20 by Kühn and
387 colleagues [7]. Similarly, the Frisén laboratory [46] used stereological and 14C quantification
388 techniques to measure cardiomyocyte exchange. They found that most cardiomyocytes were
389 never exchanged and that the substantial replacement of existing cardiomyocytes was generated
390 in the first 10 years of life, while the second decade of life focused on DNA polyploidization.
391
392 It is noteworthy to mention that in the adult murine context, approximately 85–90% of
393 cardiomyocytes exist in a binucleated state [47], indicating that the nuclear count does not precisely
394 correspond to the cell count. The polyploidization of cardiomyocytes has been recognized as an
395 impediment to heart regeneration [48]. It has been reported that binucleated cardiomyocytes re-
396 entering the cell cycle are less likely to complete cytokinesis, thereby impeding the efficient
397 regeneration of cardiac tissue following injury [36]. In adult mammalian hearts, the ratio of
398 binucleated to mononucleated cardiomyocytes varies from one species to another. In rodent
399 hearts, approximately 90% are binucleated, while in human hearts, this percentage is markedly
400 lower, varying from 25-60% [49]. Thus, a greater percentage of mononuclear cardiomyocytes in the
401 human heart would enable greater efficiency of CCNA2 gene therapy to induce cardiomyocyte
402 proliferation as a repair strategy.
403
404 Our snRNA-Seq also confirms heightened cardiomyocyte plasticity of CCNA2 transgenic mice as
405 we note changes in gene expression involved in cell cycle progression and reprogramming. Ca^{2+}

signaling is a fundamental pathway in the regulation of cell division, cardiac contractility, and remodeling [50-52]. The increase in the cytokinetic index in the test samples from 41- and 55-year-olds shows the ability of *CCNA2* to stimulate intracellular Ca^{2+} mobilization. Of note, the transduced cTnT-hCCNA2 (test samples) cultured cardiomyocytes isolated from a 21-year-old male did not show a significant increase in cytokinetic index invoked by CCNA2 when compared to the control samples, which is consistent with reports of previous investigators [7,46] that cell turnover and cell division can naturally occur at younger ages in humans.

SnRNA-seq has been used to identify transcriptomic changes occurring at the single-cell level, shedding light on the precise mapping of transcriptomic alterations in a cell-type-specific manner in response to cellular stimulation or gene delivery [53]. Employing snRNA-seq in intact tissues enables the capturing of cell-specific transcriptomics changes in a more precise manner while maintaining the integrity of tissue responses, compared to isolated *in vitro* transcriptomics analyses. Our strategy of using snRNA-seq is to identify cardiomyocyte-specific changes in an *in vivo* setting in a clinically relevant CCNA2-Tg model, which allowed us to map specific changes to a subpopulation of cardiomyocytes. This would not have been captured by analyzing the transcriptome of the bulk tissue of isolated cardiomyocytes using bulk RNA-sequencing strategies. Live-cell imaging demonstrates that CCNA2-transfected adult human cardiomyocytes successfully undergo cytokinesis, with daughter cells retaining what appear to be intact sarcomeric structures. However, transcriptomic analyses (bulk RNA-sequencing and snRNA-seq) revealed significant downregulation of sarcomere-related genes. These findings suggest a dynamic remodeling process during cytokinesis, where transcriptional downregulation of sarcomeric genes may occur transiently, while structural integrity is preserved through post-transcriptional mechanisms or protein stability. This highlights the intricate balance between cellular reprogramming and maintenance of cardiomyocyte identity during division.

Furthermore, the genes induced in the CCNA2-Tg model appear to represent a common mechanism underlying cytokinesis in both male and female mice, consistent with observations in human male and female hearts. Given that we identified a subset of cardiomyocytes that are reprogrammed into a more proliferative state, we can envision targeting this subset in future regenerative strategies. Unlike other regenerative approaches that separately target cardiomyocyte proliferation or reprogramming, our findings suggest that *CCNA2* integrates both processes, making it a unique therapeutic candidate for cardiac regeneration. Defining the transcriptomic state of cyclin A2-expressing cardiomyocytes and their proliferative potential in greater detail can enable us to recapitulate such proliferative cardiomyocytes both *in vitro* and *in vivo* to determine whether targeting these specific subpopulations holds greater therapeutic potential than targeting the entire cardiomyocyte population. The use of computational resources can aid our comprehension of these molecular mechanisms for more precision-guided regenerative strategies for human heart disease.

The ability of *CCNA2* to induce proliferation while maintaining cardiomyocyte function positions *CCNA2* gene therapy as a promising clinical approach, minimizing risks associated with exogenous cell transplantation, immune rejection, and off-target differentiation. Moreover, *CCNA2* appears to induce a transient mesenchymal-like state, as indicated by the upregulation

of *Zeb1*, a key regulator of epithelial-to-mesenchymal transition (EMT). This suggests that CCNA2-Tg cardiomyocytes adopt a plastic phenotype to facilitate cell division, similar to mechanisms observed in neonatal heart regeneration. These findings highlight *CCNA2* as a novel and safe strategy for cardiac regeneration, offering a balance between proliferative potential and structural preservation. Ongoing studies by our laboratory have revealed silencing mechanisms of endogenous CCNA2, with antisense approaches being utilized to reverse cell cycle exit and reactivate transcription of endogenous CCNA2. These approaches may offer alternative or complementary strategies to gene therapy with CCNA2.

Limitations

While the findings presented above are very promising, there are a few limitations to consider. Firstly, the use of freshly isolated human adult primary cardiomyocytes offers an ideal cellular model but presents several challenges. There is a high susceptibility to cell death in culture, which can hinder such experiments, and a fair amount of biological variability in getting the cells to adhere to the petri dishes. Adherence to the petri dishes is necessary to perform these cytokinesis experiments. Greater consistency with very rapid isolation from human cadavers and further refinements of the culture methods may overcome these challenges. Additionally, the use of adenovirus vectors is safe, and they are being utilized in other gene therapies that have been clinically tested. Immunogenicity is a concern, and therefore, there are ongoing investigations in our laboratory to explore alternative delivery strategies. Furthermore, *in vitro* models, though valuable, do not fully replicate the complexity of the *in vivo* cardiac environment. Nevertheless, this study is a valuable translational step forward from our previous preclinical report demonstrating that CCNA2 gene therapy induced a 55% increase in cardiomyocytes of the peri-infarct zones of the porcine heart [22] with significant enhancement of cardiac function. CCNA2-induced cytokinesis of human adult cardiomyocytes provides a compelling pathway toward human clinical trials of CCNA2 gene therapy for heart repair.

Methods

Culture of adult human cardiomyocytes and *in vitro* cytokinesis study

Cardiomyocytes from adult human (21-year-old male, 41-year-old female, and 55-year-old male) heart tissue were isolated after enzymatic digestion at Anabios, San Diego, CA, and were shipped to our laboratory within 24 hours of isolation. Adult human cardiomyocytes were cultured according to our previously published adult porcine cardiomyocyte culture technique [22] with slight modifications. In brief, upon arrival, cells were washed with serum-free Dulbecco's modified Eagle's medium (DMEM) (Gibco, USA) twice, and 10^5 cells were seeded in 100mm untreated polystyrene plates (Corning, USA). Non-adherent cells were collected every 24 hours and centrifuged at 20xg for 2 min at room temperature. Cell pellet was washed with serum-free DMEM and seeded on new polystyrene plates in modified Cardiomyocyte Culture Media (mod CMC) [22] formulated by adding 13% fetal bovine serum (FBS), 2.5% horse serum, 1X nonessential amino acid, 1mM sodium pyruvate, penicillin (100 U/ml), streptomycin (100 mg/ml), and fungizone (0.5 mg/ml) to DMEM/F12 (50:50). Cells were washed every day with serum-free DMEM, re-seeded

493 in new polystyrene plates and cultured for 3 days. On day 4, they were seeded in glass-bottom
494 24-well tissue culture plates for 20 days, with the medium changed every 4th day. The wells with
495 cardiomyocytes exhibiting adhesion and spreading were selected. Cells in these wells were
496 trypsinized and counted, and 10^3 cells per well were seeded in new glass-bottom tissue culture
497 plates. After 2 days of culture, cells were divided into two groups (test and control) and were
498 transduced with adenoviruses. The test group was transduced with cTnT-hCCNA2 along with
499 cTnT-eGFP and/or cTnT-H2B-GFP and CMV-α-act-mCherry adenoviruses, while the control
500 group was transduced with only cTnT-eGFP and/or cTnT-H2B-GFP and CMV-α-act-mCherry
501 adenoviruses. MOI of adenoviruses was adjusted to 180 in each well of the test (with cTnT-
502 hCCNA2; MOI 100, CMV-α-act-mCherry; MOI 40, and cTnT-eGFP or cTnT-H2B-GFP; MOI 40)
503 and the control (cTnT-eGFP; MOI 140 and CMV-α-act-mCherry; MOI 40) group. After 48 hours
504 of incubation, transduction was confirmed by observing the desired fluorescence in live cell
505 imaging with Zeiss AxioVision Observer Z1 inverted microscope (Carl Zeiss). We also tested the
506 differentiation potential (Ca^{2+} flux) of cardiomyocytes after cytokinesis *in vitro* by culturing them in
507 an agarose-based semi-solid medium for 2 weeks. Cardiomyocytes were subjected to Ca^{2+} flux
508 imaging with pacing of 0.5 Hz and 1 Hz current.
509

510 **Time-lapse microscopy**

511 To capture cell division events in cardiomyocytes *in vitro*, we carried out live cell epifluorescence
512 time-lapse microscopy as described in [22]. In brief, Zeiss AxioVision Observer Z1 (Carl Zeiss,
513 Thornwood, NY, USA) inverted epifluorescence microscope in a humidified chamber in the
514 presence of 5% CO_2 at 37°C was used to carry out time-lapse microscopy. Multiple random
515 points with cells expressing eGFP (green) and mCherry (red) were selected in the test and control
516 groups. The positions were marked with the "position-list" tool in the AxioVision microscopy
517 software (AxioVision Release 4.7, Carl Zeiss). After the first cycle of imaging, only the channel
518 for Texas red was used (for detection of mCherry) to acquire images for 72 hours. The fluorescein
519 isothiocyanate (green) channel of the microscope was kept closed during the time-lapse imaging
520 to avoid cell death from exposure to ultraviolet rays in this channel. Images were taken at intervals
521 of 30 min. The 10X objective was used for all time-lapse imaging. Time-lapse movies were
522 generated after the end of each experiment and exported as MOV files. The time-lapse movies
523 were analyzed, and cells that underwent successful cytokinesis were enumerated in each group.
524 The percentage (%) of cytokinesis events was calculated for each position, and the graph was
525 plotted.
526

527 **Cell fixation and nuclear staining**

528 After time-lapse microscopy, cells in the glass-bottom plate were fixed with 4% paraformaldehyde
529 at room temperature for 20 min and were stored at 4°C. For nuclear staining, cells were washed
530 with 1x PBS then permeabilized with 0.5% Triton X-100 solution for 20 min at room temperature.
531 Cells were washed three times with 1x PBS and incubated in DAPI solution (2.5 µg/ml) for 5 min.
532 Cells were washed twice with 1x PBS, and imaging was carried out using a Zeiss AxioVision
533 Observer Z1 inverted epifluorescence microscope.
534

535 **Real-time quantitative PCR**

Quantitative PCRs were performed in cultured cardiomyocytes transduced with cTnT-hCCNA2 (test) or cTnT-eGFP (control) adenovirus with similar MOI (MOI 100). “SYBR Green quantitative PCR protocol” on the “StepOnePlus” real-time PCR system (Applied Biosystems, CA) was used. The PCR protocol consisted of one cycle at 95°C for 2 min, 39 cycles at 95°C for 15 sec + 60°C for 1 min, and then 4°C on hold. Gene expression was determined by using the formula 2^(39-[illegible]CT) with consideration of a CT value of 39 for a single transcript and with normalization to the endogenous control *GAPDH*.

Animal

Cyclin A2 transgenic mice, adult males, and females 8-12 weeks old (n=4), were maintained in a B6CBA background [13, 19]. Non-transgenic (wild-type) littermates were used as controls (n=4).

Collection of CCNA2-Tg mouse hearts and sample preparation for single-nucleus RNA-sequencing (snRNA-seq)

Frozen heart tissues from CCNA2-Tg- and nTg adult mice, male and female, were minced and transferred into a Dounce homogenizer containing ice-cold lysis buffer (Benthos Prime Central, TX, USA). Samples were homogenized gently, and nuclei were isolated. Nuclei were ensured to be free of clumps and debris by trypan blue staining under a microscope. Nuclei were then counted, and the concentration was adjusted. 10x library concentration, insert size, and quantification were checked using Qubit, Agilent bioanalyzer, and q-PCR, respectively. For data Processing and Quality Control of 10x Sequencing of snRNA-seq, the reads were processed with 10X Genomics CellRanger software (v.3.1.0) with the default parameters for each sample. Cell Ranger employs the STAR aligner for splicing-aware mapping of reads to the genome. It utilizes a transcript annotation GTF file to categorize the reads into exonic, intronic, and intergenic regions based on whether the reads align confidently with the genome. Only confidently mapped, non-PCR duplicates with valid barcodes and UMIs were used to generate a gene-barcode matrix. This involved various steps, including alignment to a reference, collapsing of unique molecular identifiers (UMIs), UMI counting, and initial quality control procedures. The output of this process was the generation of filtered gene expression matrices that exclusively contained cellular barcodes. Subsequently, the Seurat R package (v.3.1.1) was used for data quality control and downstream processing. The filtered_feature_bc_matrix generated by Cell Ranger was used for Seurat processing. Post-sequencing quality control was performed using Seurat. Cells were excluded from downstream processing in each sample if they met any of the following criteria: fewer than 200 genes were detected per cell, genes had non-zero counts in at most three cells, total feature counts exceeded 8000 (suggesting potential multiplets), more than 50% of the feature count was attributable to mitochondrial genes, or more than 5% of the feature count was attributable to hemoglobin-related genes, and doublets from all the clusters were filtered during QC using DoubletFinder version 2.0.3 **(Figure S2)**. Raw read counts were log-normalized, cells were clustered, and markers for each cluster were identified by using the Seurat FindMarkers and FindAllMarker functions [54]. The cell clusters were annotated by using iRhythmics FairdomHub instance (https://fairdomhub.org/studies/739) and prior knowledge.

Human fetal and adult hearts and RNA sequencing

579 Human fetal heart RNA (n=3 pooled, Cat #636532, Takara) and human adult heart RNA (n=4
580 pooled, Cat #636583, Takara) were used for bulk RNA sequencing with an increased read depth
581 (Ultra-deep sequencing), generating approximately 300 million reads per sample. This high
582 sequencing depth enabled the detection of rare transcripts, improved quantification accuracy,
583 and enhanced the resolution of transcript isoforms, including novel and unannotated RNAs. For
584 library preparation, we employed a ribosomal RNA (rRNA) depletion strategy instead of poly(A)
585 enrichment to capture both polyadenylated (polyA$^+$) and non-polyadenylated (polyA$^-$) RNAs.
586 While polyA$^+$ selection primarily enriches for mRNAs and some lncRNAs, rRNA depletion allows
587 for the inclusion of a broader spectrum of regulatory RNAs, including enhancer RNAs (eRNAs),
588 small nuclear RNAs (snRNAs), and uncharacterized lncRNAs that may lack poly(A) tails.
589 Additionally, this approach reduces transcript bias, preserves isoform diversity, and is better
590 suited for degraded RNA samples.
591 By combining rRNA depletion with ultra-deep sequencing, we achieved a comprehensive and
592 unbiased profile of the cardiac transcriptome. The sequence reads were mapped to the human
593 genome (GRCh38.110) using STAR [55] (version 2.7.9a). Using the mapped reads, the R package
594 edgeR [56] (version 3.30.3) was employed to calculate counts per million (CPM) values and false
595 discovery rate (FDR)-adjusted p-values obtained through the Benjamini–Hochberg method
596 (Benthos Prime Central, TX, USA).
597

598 **Pathway enrichment analysis**

599 Pathway enrichment analysis was performed using the Reactome pathway analysis tool [57]. The
600 differentially expressed genes among nTg and CCNA2-Tg conditions (log2FC > / < 1 and a P
601 value < 0.05) were used for pathway analysis. Fold enrichment was calculated to indicate the
602 gene expression observed in our list compared to the expected list. Categories with a fold
603 enrichment greater than 1 were considered overrepresented, while those with a fold enrichment
604 less than 1 were considered underrepresented in our experiment. Additionally, pathway
605 enrichment analysis was conducted using BioPlanet via the EnrichR suite [58], following a
606 previously described approach [59].
607

608 **Statistical analysis**

609 Statistical analyses were carried out using the R package (version 3.30.3), GraphPad Prism
610 (version 8.2.1, GraphPad), and Python (via Google Colab). Two-tailed unpaired or paired *t*-tests
611 were used for comparison between groups with normally distributed data. Chi-square (χ^2) tests
612 for proportions were performed using Python libraries, including *Scipy*. The sample size (n) is
613 reported for each analysis. Data are presented as means ± s.e.m unless otherwise indicated.
614 Statistical significance was defined as P < 0.05.
615

616 **Study approval**

617 This study was conducted in accordance with the Declaration of Helsinki. Adult human
618 cardiomyocytes were obtained from Anabios (San Diego, CA) and were fully de-identified, and
619 therefore are exempt from ethics approval. For the mouse study, the protocol was approved by
620 the Institutional Animal Care and Use Committee (IACUC) of Mount Sinai Hospital, and all
621 procedures adhered to Institutional Animal Care and Use Guidelines.
622

Data availability

The processed single-nucleus data and the deep bulk RNA sequencing, including raw expression matrices and raw sequence files that support this research study's findings, are available on the Gene Expression Omnibus GSE249433 and GSE256519, respectively.

Article Information

Author Contributions

E.B. wrote the original article, contributed to experiments, and analyzed and performed snRNA-seq data with input from P.M. and A.K.; S.V.M and A.K.R contributed to cytokinesis experiments and calcium measurements; P.M. contributed to processing snRNA-seq samples and initial analysis with assistance from AK; C.D.S. assisted with the cell biology experiments and organization of the manuscript; P.E.M., A.G., N.A.G. provided cardiomyocytes through their proprietary technology. H.W.C. was responsible for conceptualization, vector design, validation, supervision, reviewing, and funding acquisition. Review & editing- E.B, H.W.C, P.M., and A.K.

Acknowledgment

We thank Dr. Bernhard Kühn for his contribution to the cTnT-H2B-GFP utilized in this study.This work was supported by the National Institutes of Health National Heart, Lung, and Blood Institute (NIH R01 HL150345), the New York Stem Cell Science (NYSTEM C029565 and C32608GG).

Competing interests

H.W.C. is the inventor of multiple patents regarding cyclin A2-mediated cardiac repair and caudal-related homeobox 2 cells for cardiac repair. She is in the midst of launching a new biotechnology company to advance such therapies to clinical development. Other authors declare no financial competing interests.

Abbreviations and Acronyms	
Actn2	Actinin Alpha 2
Atp2a2	ATPase, SERCA2
Atp5b	ATP Synthase, Mitochondrial F1 Complex, Beta Polypeptide ATP
Atp5g3	Synthase, Mitochondrial C Subunit, Gamma Polypeptide 3
Bub1	BUB1 Mitotic Checkpoint Serine/Threonine Kinase
C1qa	Complement C1q A Chain
Ca^{2+}	Calcium ion
Calm1	Calmodulin 1
Calm2	Calmodulin 2
CCNA2	Cyclin A2
CCNA2-Tg	CCNA2- transgenic mice
Cdc20	Cell Division Cycle 20
Cdk1	Cyclin-Dependent Kinase 1
Cdk2	Cyclin-Dependent Kinase 2
CGC	Cardiac glial cells
CMs	Cardiomyocytes
CPM	Counts per million
CTnT	Cardiac Troponin T
CTnT-hCCNA2	Cardiac Troponin T- human cyclin A2
E1/E2	Early region 1/Early region 2
EC	Endothelial cells
EC-derived FB	Endothelial-derived fibroblasts
EDC	Endocardial cells
Efnb2	Ephrin B2
eGFP	Enhanced Green Fluorescent Protein
EPC	Epicardial cells
EP-derived FB	Epicardial derived fibroblasts
ES	Embryonic stem cells
FB	Fibroblasts
FDR	False discovery rate
Gata4	GATA Binding Protein 4
H2B	Histone 2B
Igfbp3	Insulin-Like Growth Factor Binding Protein 3
iPS	Induced pluripotent
Kcnd2	Potassium Voltage-Gated Channel Subfamily D Member 2
Kif23	Kinesin Family Member 23
Klf4	Kruppel Like Factor 4
MI	Myocardial infarction
Mki67	Marker of Proliferation Ki-67
MOI	Multiplicity of Infection
Mono	Monocytes
Myc	MYC Proto-Oncogene, BHLH Transcription Factor
Myh7	Myosin Heavy Chain 7
Myl2	Myosin Light Chain 2

Myob	Myoblasts
NC	Neuronal cells
Neb	Nebulin
nTg	Non-transgenic mice
PEC	Pericytes
Pkp2	Plakophilin 2
Pln	Phospholamban
Pou5f1	POU Class 5 Homeobox 1, Oct4
Prc1	Protein Regulator of Cytokinesis 1
Pro-vCM	Proliferative ventricular cardiomyocyte
Ryr2	Ryanodine Receptor 2
Scn5a	Sodium Voltage-Gated Channel Alpha Subunit 5
SMC	Smooth muscle cells
SnRNA-seq	Single nucleus RNA sequencing
TC	T-Cells
Tnnc1	Troponin C1
Tnni3k	Troponin I Interacting Kinase
Top2a	Topoisomerase (DNA) II Alpha
t-SNE	T-distributed Stochastic Neighbor Embedding
Ttn	Titin
UMI	Unique molecular identifier
UnkC	Unknown cells
vCM	Ventricular cardiomyocyte
VEC	Vascular endothelial cells
α-act	Alpha-actinin

650
651

652 ## References

653 1 Yoshizumi, M. *et al.* Disappearance of cyclin A correlates with permanent withdrawal of
654 cardiomyocytes from the cell cycle in human and rat hearts. *J Clin Invest* **95**, 2275-2280
655 (1995). https://doi.org/10.1172/JCI117918
656 2 Miyamoto, K. *et al.* Direct In Vivo Reprogramming with Sendai Virus Vectors Improves
657 Cardiac Function after Myocardial Infarction. *Cell Stem Cell* **22**, 91-103 e105 (2018).
658 https://doi.org/10.1016/j.stem.2017.11.010
659 3 Doppler, S. A. *et al.* Mammalian Heart Regeneration: The Race to the Finish Line. *Circ*
660 *Res* **120**, 630-632 (2017). https://doi.org/10.1161/CIRCRESAHA.116.310051
661 4 Yoshida, Y. & Yamanaka, S. Induced Pluripotent Stem Cells 10 Years Later: For Cardiac
662 Applications. *Circ Res* **120**, 1958-1968 (2017).
663 https://doi.org/10.1161/CIRCRESAHA.117.311080
664 5 Shiba, Y. *et al.* Allogeneic transplantation of iPS cell-derived cardiomyocytes regenerates
665 primate hearts. *Nature* **538**, 388-391 (2016). https://doi.org/10.1038/nature19815
666 6 Chong, J. J. *et al.* Human embryonic-stem-cell-derived cardiomyocytes regenerate non-
667 human primate hearts. *Nature* **510**, 273-277 (2014). https://doi.org/10.1038/nature13233
668 7 Mollova, M. *et al.* Cardiomyocyte proliferation contributes to heart growth in young
669 humans. *Proc Natl Acad Sci U S A* **110**, 1446-1451 (2013).
670 https://doi.org/10.1073/pnas.1214608110
671 8 Bergmann, O. *et al.* Evidence for cardiomyocyte renewal in humans. *Science* **324**, 98-102
672 (2009). https://doi.org/10.1126/science.1164680
673 9 Brockes, J. P. & Kumar, A. Plasticity and reprogramming of differentiated cells in
674 amphibian regeneration. *Nat Rev Mol Cell Biol* **3**, 566-574 (2002).
675 https://doi.org/10.1038/nrm881
676 10 Poss, K. D., Wilson, L. G. & Keating, M. T. Heart regeneration in zebrafish. *Science* **298**,
677 2188-2190 (2002). https://doi.org/10.1126/science.1077857
678 11 Jopling, C. *et al.* Zebrafish heart regeneration occurs by cardiomyocyte dedifferentiation
679 and proliferation. *Nature* **464**, 606-609 (2010). https://doi.org/10.1038/nature08899
680 12 Furtado, M. B., Nim, H. T., Boyd, S. E. & Rosenthal, N. A. View from the heart: cardiac
681 fibroblasts in development, scarring and regeneration. *Development* **143**, 387-397 (2016).
682 https://doi.org/10.1242/dev.120576
683 13 Chaudhry, H. W. *et al.* Cyclin A2 mediates cardiomyocyte mitosis in the postmitotic
684 myocardium. *J Biol Chem* **279**, 35858-35866 (2004).
685 https://doi.org/10.1074/jbc.M404975200
686 14 Nurse, P. A long twentieth century of the cell cycle and beyond. *Cell* **100**, 71-78 (2000).
687 https://doi.org/10.1016/s0092-8674(00)81684-0
688 15 Pagano, M., Pepperkok, R., Verde, F., Ansorge, W. & Draetta, G. Cyclin A is required at
689 two points in the human cell cycle. *EMBO J* **11**, 961-971 (1992).
690 https://doi.org/10.1002/j.1460-2075.1992.tb05135.x
691 16 Sherr, C. J. & Roberts, J. M. Inhibitors of mammalian G1 cyclin-dependent kinases. *Genes*
692 *Dev* **9**, 1149-1163 (1995). https://doi.org/10.1101/gad.9.10.1149
693 17 Wang, B. J. & Chaudhry, H. W. Regulation of Cardiomyocyte Division During Cardiac
694 Regeneration. *Curr Cardiol Rep* **25**, 615-620 (2023). https://doi.org/10.1007/s11886-023-
695 01886-7
696 18 Vadakke-Madathil, S. & Chaudhry, H. W. Cardiac Regeneration: Time to Revisit Nature.
697 *Circ Res* **123**, 24-26 (2018). https://doi.org/10.1161/CIRCRESAHA.118.313246

19 Cheng, R. K. *et al.* Cyclin A2 induces cardiac regeneration after myocardial infarction and prevents heart failure. *Circ Res* **100**, 1741-1748 (2007). https://doi.org/10.1161/CIRCRESAHA.107.153544

20 Woo, Y. J. *et al.* Therapeutic delivery of cyclin A2 induces myocardial regeneration and enhances cardiac function in ischemic heart failure. *Circulation* **114**, I206-213 (2006). https://doi.org/10.1161/CIRCULATIONAHA.105.000455

21 Woo, Y. J. *et al.* Myocardial regeneration therapy for ischemic cardiomyopathy with cyclin A2. *J Thorac Cardiovasc Surg* **133**, 927-933 (2007). https://doi.org/10.1016/j.jtcvs.2006.07.057

22 Shapiro, S. D. *et al.* Cyclin A2 induces cardiac regeneration after myocardial infarction through cytokinesis of adult cardiomyocytes. *Sci Transl Med* **6**, 224ra227 (2014). https://doi.org/10.1126/scitranslmed.3007668

23 Litvinukova, M. *et al.* Cells of the adult human heart. *Nature* **588**, 466-472 (2020). https://doi.org/10.1038/s41586-020-2797-4

24 Bak, S. T. *et al.* Ploidy-stratified single cardiomyocyte transcriptomics map Zinc Finger E-Box Binding Homeobox 1 to underly cardiomyocyte proliferation before birth. *Basic Res Cardiol* **118**, 8 (2023). https://doi.org/10.1007/s00395-023-00979-2

25 So, J. *et al.* Robust single-nucleus RNA sequencing reveals depot-specific cell population dynamics in adipose tissue remodeling during obesity. *Elife* **13** (2025). https://doi.org/10.7554/eLife.97981

26 Galow, A. M. *et al.* Quality control in scRNA-Seq can discriminate pacemaker cells: the mtRNA bias. *Cell Mol Life Sci* **78**, 6585-6592 (2021). https://doi.org/10.1007/s00018-021-03916-5

27 Galow, A. M. *et al.* Integrative Cluster Analysis of Whole Hearts Reveals Proliferative Cardiomyocytes in Adult Mice. *Cells* **9** (2020). https://doi.org/10.3390/cells9051144

28 Lai, Z. F. *et al.* Overexpression of TNNI3K, a cardiac-specific MAP kinase, promotes P19CL6-derived cardiac myogenesis and prevents myocardial infarction-induced injury. *Am J Physiol Heart Circ Physiol* **295**, H708-716 (2008). https://doi.org/10.1152/ajpheart.00252.2008

29 Rajakumari, S. *et al.* EBF2 determines and maintains brown adipocyte identity. *Cell Metab* **17**, 562-574 (2013). https://doi.org/10.1016/j.cmet.2013.01.015

30 Wang, L. *et al.* Polymorphisms of the tumor suppressor gene LSAMP are associated with left main coronary artery disease. *Ann Hum Genet* **72**, 443-453 (2008). https://doi.org/10.1111/j.1469-1809.2008.00433.x

31 Liu, J. *et al.* Aberrantly high activation of a FoxM1-STMN1 axis contributes to progression and tumorigenesis in FoxM1-driven cancers. *Signal Transduct Target Ther* **6**, 42 (2021). https://doi.org/10.1038/s41392-020-00396-0

32 Zhao, L. *et al.* CD44 regulates vascular gene expression in a proatherogenic environment. *Arterioscler Thromb Vasc Biol* **27**, 886-892 (2007). https://doi.org/10.1161/01.ATV.0000259362.10882.c5

33 Beisaw, A. & Wu, C. C. Cardiomyocyte maturation and its reversal during cardiac regeneration. *Dev Dyn* **253**, 8-27 (2024). https://doi.org/10.1002/dvdy.557

34 Xing, Z. *et al.* Expression and prognostic value of CDK1, CCNA2, and CCNB1 gene clusters in human breast cancer. *J Int Med Res* **49**, 300060520980647 (2021). https://doi.org/10.1177/0300060520980647

35 Santamaria, D. *et al.* Cdk1 is sufficient to drive the mammalian cell cycle. *Nature* **448**,

744 811-815 (2007). https://doi.org/10.1038/nature06046
745 36 Bersell, K., Arab, S., Haring, B. & Kuhn, B. Neuregulin1/ErbB4 signaling induces
746 cardiomyocyte proliferation and repair of heart injury. *Cell* **138**, 257-270 (2009).
747 https://doi.org/10.1016/j.cell.2009.04.060
748 37 Leeuwenburgh, B. P. *et al.* Chronic right ventricular pressure overload results in a
749 hyperplastic rather than a hypertrophic myocardial response. *J Anat* **212**, 286-294 (2008).
750 https://doi.org/10.1111/j.1469-7580.2008.00853.x
751 38 Assey, M. E., Wisenbaugh, T., Spann, J. F., Jr., Gillette, P. C. & Carabello, B. A.
752 Unexpected persistence into adulthood of low wall stress in patients with congenital aortic
753 stenosis: is there a fundamental difference in the hypertrophic response to a pressure
754 overload present from birth? *Circulation* **75**, 973-979 (1987).
755 https://doi.org/10.1161/01.cir.75.5.973
756 39 Torp, K. H. Congenital aortic stenosis with hyperplasia of the endocardium in the left
757 ventricle. *Acta Pathol Microbiol Scand* **29**, 109-119 (1951). https://doi.org/10.1111/j.1699-
758 0463.1951.tb00109.x
759 40 Kranenburg, O., van der Eb, A. J. & Zantema, A. Cyclin D1 is an essential mediator of
760 apoptotic neuronal cell death. *EMBO J* **15**, 46-54 (1996).
761 41 Freeman, R. S., Estus, S. & Johnson, E. M., Jr. Analysis of cell cycle-related gene
762 expression in postmitotic neurons: selective induction of Cyclin D1 during programmed
763 cell death. *Neuron* **12**, 343-355 (1994). https://doi.org/10.1016/0896-6273(94)90276-3
764 42 Sofer-Levi, Y. & Resnitzky, D. Apoptosis induced by ectopic expression of cyclin D1 but
765 not cyclin E. *Oncogene* **13**, 2431-2437 (1996).
766 43 Kong, G. *et al.* Functional analysis of cyclin D2 and p27(Kip1) in cyclin D2 transgenic
767 mouse mammary gland during development. *Oncogene* **21**, 7214-7225 (2002).
768 https://doi.org/10.1038/sj.onc.1205895
769 44 Liu, Y. & Kitsis, R. N. Induction of DNA synthesis and apoptosis in cardiac myocytes by
770 E1A oncoprotein. *J Cell Biol* **133**, 325-334 (1996). https://doi.org/10.1083/jcb.133.2.325
771 45 Wang, J., Chenivesse, X., Henglein, B. & Brechot, C. Hepatitis B virus integration in a
772 cyclin A gene in a hepatocellular carcinoma. *Nature* **343**, 555-557 (1990).
773 https://doi.org/10.1038/343555a0
774 46 Bergmann, O. *et al.* Dynamics of Cell Generation and Turnover in the Human Heart. *Cell*
775 **161**, 1566-1575 (2015). https://doi.org/10.1016/j.cell.2015.05.026
776 47 Soonpaa, M. H., Kim, K. K., Pajak, L., Franklin, M. & Field, L. J. Cardiomyocyte DNA
777 synthesis and binucleation during murine development. *Am J Physiol* **271**, H2183-2189
778 (1996). https://doi.org/10.1152/ajpheart.1996.271.5.H2183
779 48 Gonzalez-Rosa, J. M. *et al.* Myocardial Polyploidization Creates a Barrier to Heart
780 Regeneration in Zebrafish. *Dev Cell* **44**, 433-446 e437 (2018).
781 https://doi.org/10.1016/j.devcel.2018.01.021
782 49 Botting, K. J. *et al.* Early origins of heart disease: low birth weight and determinants of
783 cardiomyocyte endowment. *Clin Exp Pharmacol Physiol* **39**, 814-823 (2012).
784 https://doi.org/10.1111/j.1440-1681.2011.05649.x
785 50 Patergnani, S. *et al.* Various Aspects of Calcium Signaling in the Regulation of Apoptosis,
786 Autophagy, Cell Proliferation, and Cancer. *Int J Mol Sci* **21** (2020).
787 https://doi.org/10.3390/ijms21218323
788 51 Rosendo-Pineda, M. J., Moreno, C. M. & Vaca, L. Role of ion channels during cell
789 division. *Cell Calcium* **91**, 102258 (2020). https://doi.org/10.1016/j.ceca.2020.102258

790 52 Liu, C. *et al.* Alteration of calcium signalling in cardiomyocyte induced by simulated
791 microgravity and hypergravity. *Cell Prolif* **53**, e12783 (2020).
792 https://doi.org/10.1111/cpr.12783
793 53 Bode, D., Cull, A. H., Rubio-Lara, J. A. & Kent, D. G. Exploiting Single-Cell Tools in
794 Gene and Cell Therapy. *Front Immunol* **12**, 702636 (2021).
795 https://doi.org/10.3389/fimmu.2021.702636
796 54 Koenig, A. L. *et al.* Single-cell transcriptomics reveals cell-type-specific diversification in
797 human heart failure. *Nat Cardiovasc Res* **1**, 263-280 (2022).
798 https://doi.org/10.1038/s44161-022-00028-6
799 55 Dobin, A. *et al.* STAR: ultrafast universal RNA-seq aligner. *Bioinformatics* **29**, 15-21
800 (2013). https://doi.org/10.1093/bioinformatics/bts635
801 56 Robinson, M. D., McCarthy, D. J. & Smyth, G. K. edgeR: a Bioconductor package for
802 differential expression analysis of digital gene expression data. *Bioinformatics* **26**, 139-
803 140 (2010). https://doi.org/10.1093/bioinformatics/btp616
804 57 Fabregat, A. *et al.* Reactome pathway analysis: a high-performance in-memory approach.
805 *BMC Bioinformatics* **18**, 142 (2017). https://doi.org/10.1186/s12859-017-1559-2
806 58 Xie, Z. *et al.* Gene Set Knowledge Discovery with Enrichr. *Curr Protoc* **1**, e90 (2021).
807 https://doi.org/10.1002/cpz1.90
808 59 Huang, R. *et al.* The NCATS BioPlanet - An Integrated Platform for Exploring the
809 Universe of Cellular Signaling Pathways for Toxicology, Systems Biology, and Chemical
810 Genomics. *Front Pharmacol* **10**, 445 (2019). https://doi.org/10.3389/fphar.2019.00445
811
812

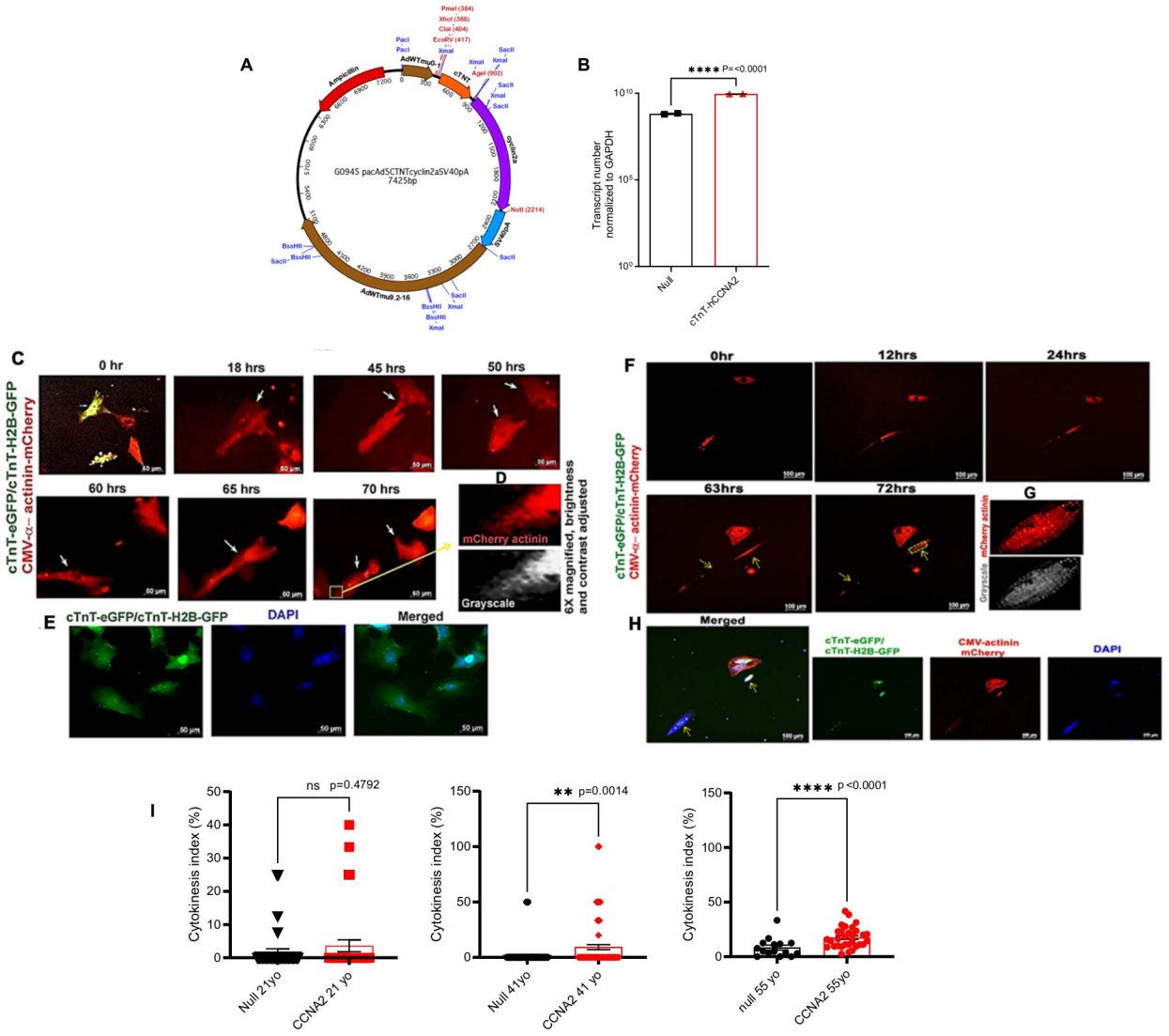

Figure 1. CCNA2 expression induces cytokinesis in adult human cardiomyocytes *In Vitro*. **A)** Clinical-use grade replication-deficient human adenovirus type 5 (Ad5) was used for this study. The vector was designed with cardiac Troponin T (cTnT) promoter to express human cyclin A2 (hCCNA2) specifically in cardiomyocytes. **B)** The cTnT-hCCNA2 adenovirus was used to transduce cultured adult human cardiomyocytes to induce the expression of CCNA2. Significantly higher CCNA2 expression was observed in cells transduced with cTnT-hCCNA2 compared to the control virus. **C-H)** Still images from representative time-lapse epifluorescence microscopy of cultured cardiomyocytes isolated from adult humans **C**) 55-year-old and **F)** 41-year-old. Please note that still images of 55 and 41-years-old have scale bars of 50µm and 100µm as it is shown in the movies S1 and S2 respectively. Cells were transduced with cTnT-hCCNA2, cTnT-H2B-GFP, cTnT-eGFP (to label cardiomyocytes), and CMV-α-actinin-m-Cherry adenoviruses prior to the beginning of the time-lapse imaging. **C)** At time 0 hr, a cell (yellow) expressing both cTnT (green) and α-actinin (red) was followed for 70 hrs via time-lapse microscopy. The green channel was closed, and cells were only followed through the red channel to avoid UV photo-toxicity. The observed human cardiomyocytes show the 1st cell division at 50 hrs of imaging, and one of the daughter cells subsequently undergoes division at 70 hrs of imaging. **D** and **G)** At 70/72 hrs, a

832 daughter cell is partially magnified with a grayscale version to demonstrate the presence of an
833 intact sarcomere structure. **E, H)** 1 day after live imaging ended, these wells were fixed with
834 subsequent labeling of nuclei with DAPI. The green fluorescence of the original cTnT-eGFP and
835 cTnT-H2B-GFP transduction is visible, further confirming that these cells are cardiomyocytes. **I)**
836 The cytokinetic events were counted in the control and test samples from the 21-, 41-, and 55-
837 year-old subjects. A significantly higher rate of cytokinesis was observed in the test samples from
838 the 41-year-old (p=0.001) and 55-year-old (p<0.0001) compared to the control. On the other
839 hand, the control and test samples from the 21-year-old did not exhibit a significant difference in
840 cytokinetic events (p=0.47). Data are represented as mean ± s.e.m.
841

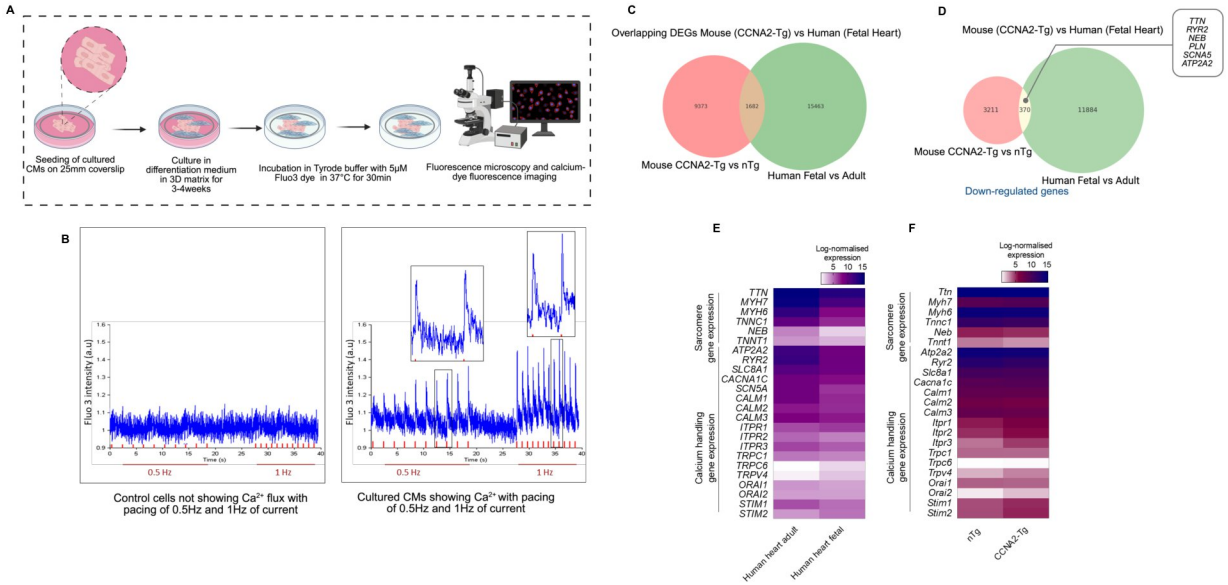

Figure 2. Differentiation of cultured adult human cardiomyocytes. Cultured adult human cardiomyocytes typically undergo dedifferentiation and were then subjected to 3D redifferentiation culture conditions and examined for Ca^{2+} flux. **A)** Overview of the 3D culture method of differentiation, Ca^{2+} flux measurement, and fluorescence microscopy in adult human cardiomyocytes. **B)** Representative Ca^{2+} flux graphs of re-differentiated cultured adult human cardiomyocytes. Ad5-cTnT-hCCNA2 transduced adult human cardiomyocytes show Ca^{2+} flux with pacing of 0.5 and 1 Hz of current, while no Ca^{2+} flux was detected in the non-Ad5-cTnT-hCCNA2 transduced cardiomyocytes. **C)** Venn diagram showing the overlap of differentially expressed genes between CCNA2-Tg versus non-nTg mouse cardiomyocytes and human fetal versus adult hearts. **D)** Venn diagram displaying the subset of downregulated genes shared between the CCNA2-Tg mouse hearts and the fetal human heart. These genes include several associated with cardiomyocyte maturation. **E)** Heatmap depicting the expression of Ca^{2+} handling, contractility, and sarcomere-associated genes in human adult versus fetal hearts, **F)** Comparison of gene expression in cardiomyocytes from CCNA2-Tg versus nTg mice, highlighting differences in Ca^{2+} regulatory genes and contractile machinery. Positive values indicate upregulation in adult hearts relative to fetal hearts. Data represent normalized RNA-sequencing expression values. The illustration in (**A**) was created using BioRender (https://biorender.com).

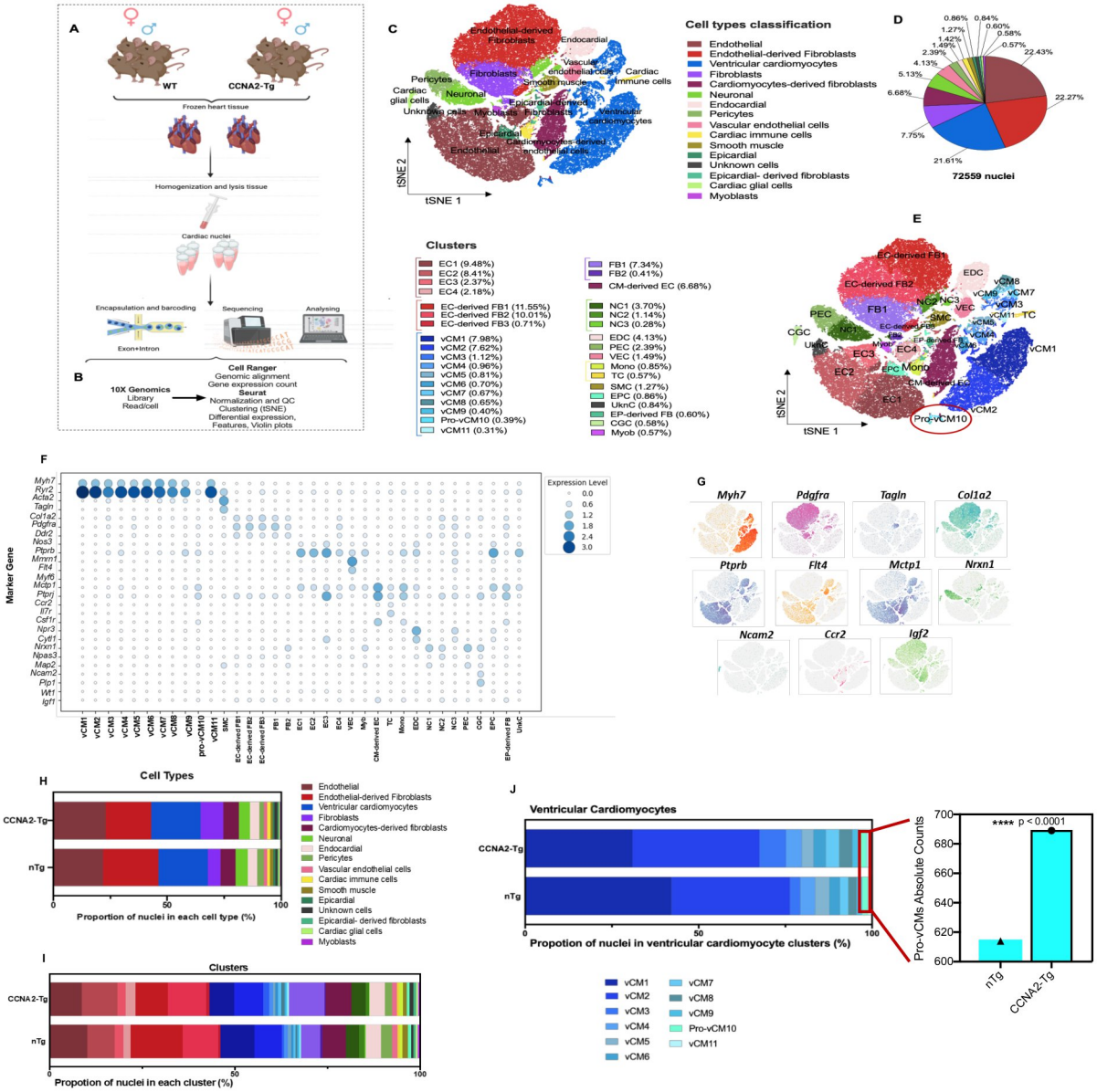

Figure 3. Single-nucleus RNA sequencing identified major cell types in CCNA2-Tg mice
A) Schematic depicting the design of the snRNA-seq experiments (n=2) for each condition nTg female, CCNA2-Tg female, nTg male, and nTg male. (*n*= 8 mice in total). **B)** The analysis pipeline and single-cell barcoded library generation (10X Genomics), sequence alignment (Cell Ranger), and further analysis using R (SeuratR package). (*n*= total nuclei 72,559) **C)** t-distributed Stochastic Neighbor Embedding (t-SNE) clustering the nuclei reveals more than 16 distinct major cell types identified based on the cell-specific markers dataset provided at iRhythmics FairdomHub instance, and **D)** the pie chart showing the proportion of cells within the snRNA-seq. **E)** t-SNE of a total of 35 subclusters. **F)** Dot plot depicting the expression levels of some of the key marker genes used to classify cell types. Dot size represents the percentage of cells expressing each gene, while color intensity reflects expression levels. **G)** Feature plots highlighting the expression of selected cell-type-specific markers across the t-SNE space. **H)** Stacked bar plots representing the proportion of nuclei classified into each major cell type (top) and **I)** each identified cluster (bottom) in both CCNA2-Tg and nTg mice. **J)** Stacked bar plots

879 displaying the proportion of nuclei in vCM clusters (left). The absolute count comparison (right)
880 highlights a significant increase in Pro-vCM10 in CCNA2-Tg hearts relative to nTg controls (****p
881 < 0.0001, Chi-square test), supporting the role of CCNA2 in promoting cardiomyocyte
882 proliferation. CM: Cardiomyocytes, vCM: ventricular cardiomyocytes, EC: endothelial cells, FB:
883 fibroblasts, EC-derived FB: endothelial-derived fibroblasts, NC: neuronal, EDC: endocardial cells.
884 PEC: pericytes, VEC: vascular endothelial cells, Mono: monocytes, TC: T-Cells, SMC: smooth
885 muscle cells, EPC: epicardial cells, UnkC: unknown cells, EP-derived FB: epicardial-derived
886 fibroblasts, CGC: Cardiac glial cells, Myob: myoblasts. The illustration in (**A**) was created using
887 BioRender (https://biorender.com).

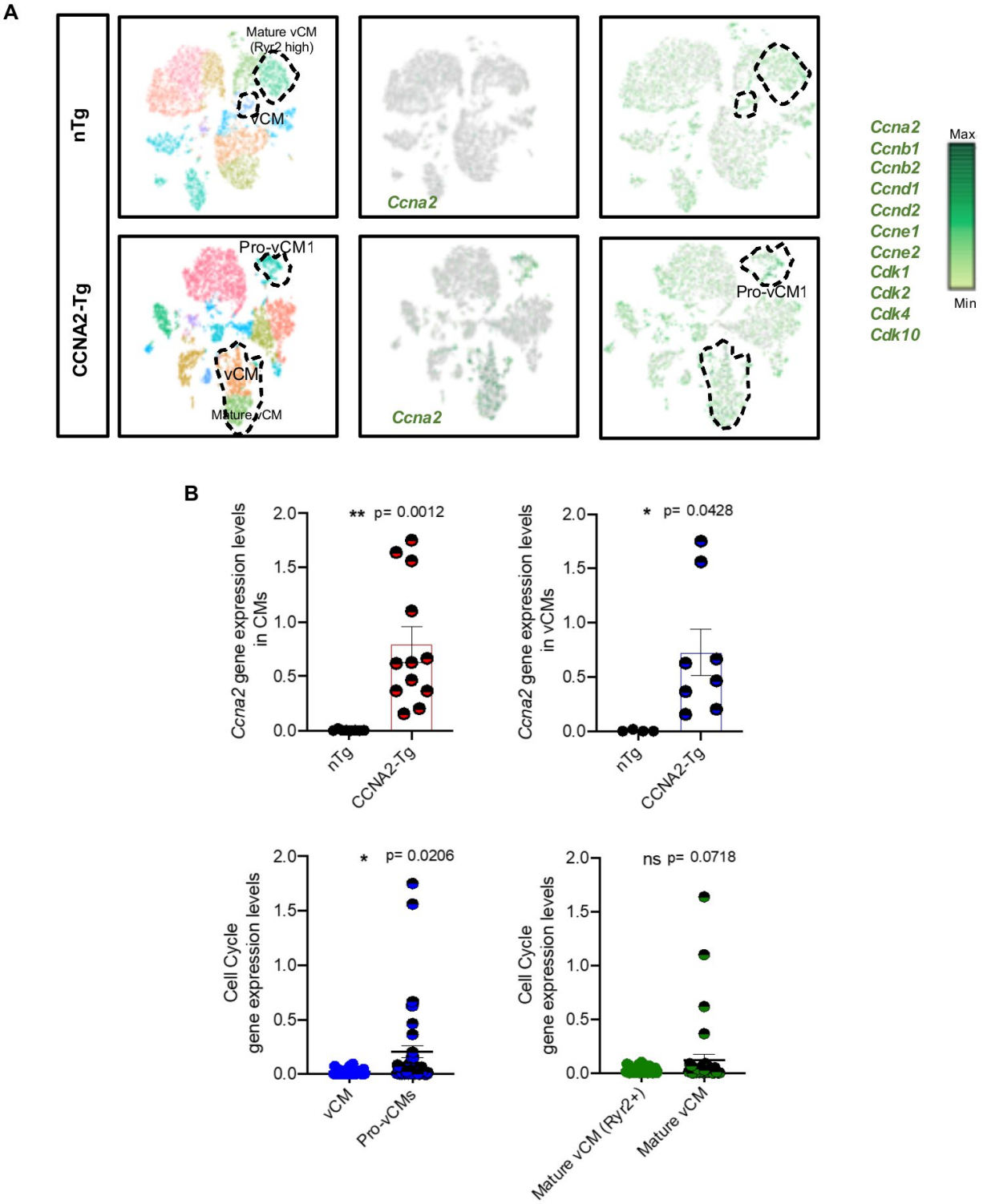

Figure 4. CCNA2 and cell cycle genes expression in CCNA2-Tg and nTg mice cardiomyocytes delineated by snRNA-seq. A) CCNA2 was expressed in the vCM, specifically

891 in the pro-vCM subset of the cardiomyocyte population in CCNA2-Tg, and cell cycle genes
892 projected on the t-SNE plot. **B)** Scatter plots showing the expression level of CCNA2 and cell
893 cycle genes in cardiomyocytes of CCNA2-Tg and nTg mice. Each point represents an individual
894 value; the mean value is represented by the horizontal line. Error bars represent s.e.m.
895

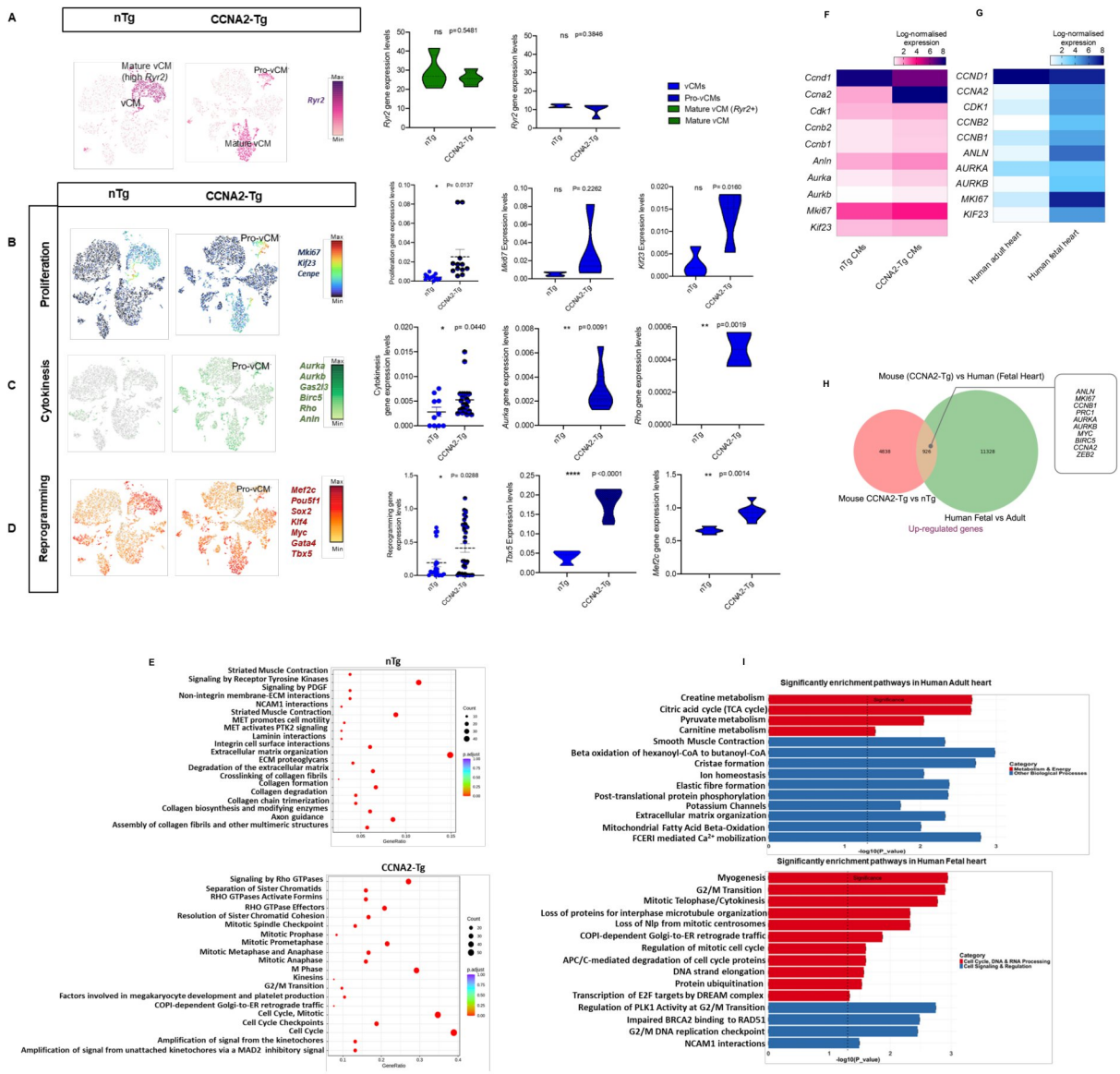

Figure 5. CCNA2 expression induces proliferation, cytokinesis, and reprogramming in mouse cardiomyocytes. A) t-SNE projection showing *Ryr2* expression across cardiomyocyte subpopulations in nTg and CCNA2-Tg mice. *Ryr2*+ cardiomyocytes correspond to a more mature ventricular cardiomyocyte (vCM) state, whereas *Ryr2* low expression cardiomyocytes represent less mature, or proliferative cardiomyocytes. Quantification of *Ryr2* expression levels among cardiomyocyte subpopulations is shown in the accompanying violin plot, highlighting differences in *Ryr2* expression across conditions. **B)** t-SNE plots and representative scatter plots and Violin plots representing the expression of key proliferation, **C)** cytokinesis, and **D)** reprogramming gene markers in both CCNA2-Tg and nTg mice. **E)** Representative dot plot of the differential gene expression analysis showing the upregulation of proliferation, cytokinesis, and reprogramming genes in CCNA2-Tg versus nTg cardiomyocytes. **F)** Heatmaps of log-transformed gene expression changes in human fetal versus adult hearts, **G)** and in CCNA2-Tg versus nTg cardiomyocytes. **H)** Venn diagram showing shared upregulated genes between CCNA2-

912 transgenic mouse hearts and human fetal hearts. The diagram displays the overlap of upregulated
913 genes from CCNA2-Tg versus non-nTg mouse cardiomyocytes and human fetal versus adult
914 heart RNA-seq datasets. These shared genes are further associated with cell cycle, cytokinesis,
915 and cardiac development, supporting a dedifferentiation and reprogramming phenotype induced
916 by CCNA2. **I)** Pathway enrichment analysis showing significantly enriched pathways in human
917 adult (top) and fetal (bottom) heart. In the adult heart, pathways related to metabolism and energy
918 are enriched, based on 4,348 downregulated genes and 3,713 upregulated genes ($P<0.05$). In
919 the fetal heart, cell cycle, DNA/RNA processing, and signaling pathways are enriched ($P<0.05$).

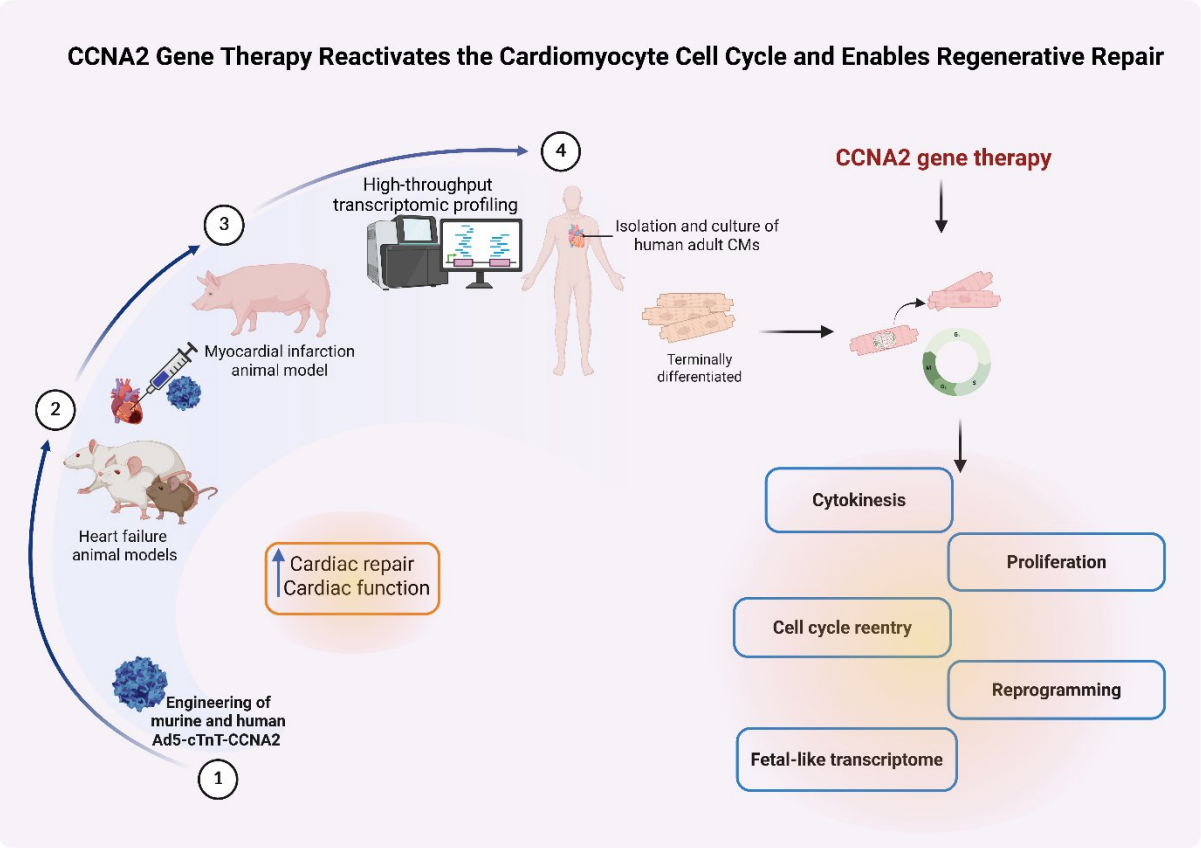

Figure 6. Translational roadmap and mechanistic model of CCNA2 gene therapy for cardiac regeneration. Building upon our previous *in vivo* studies in rodent and porcine myocardial infarction models, which demonstrated functional recovery via CCNA2 gene therapy (1-3) [19-22], this study provides direct evidence of complete cytokinesis in cultured human adult cardiomyocytes. Complementary transcriptomic analyses from fetal and adult human hearts, as well as CCNA2 transgenic models, reveal reactivation of fetal-like, proliferative, and reprogramming gene programs. The schematic illustrates the translational trajectory from preclinical to mechanistic insights and highlights CCNA2 as a driver of cardiomyocyte cell cycle reentry, cytokinesis, and regenerative gene expression. The illustration was created using BioRender (https://biorender.com).

Supplemental Material

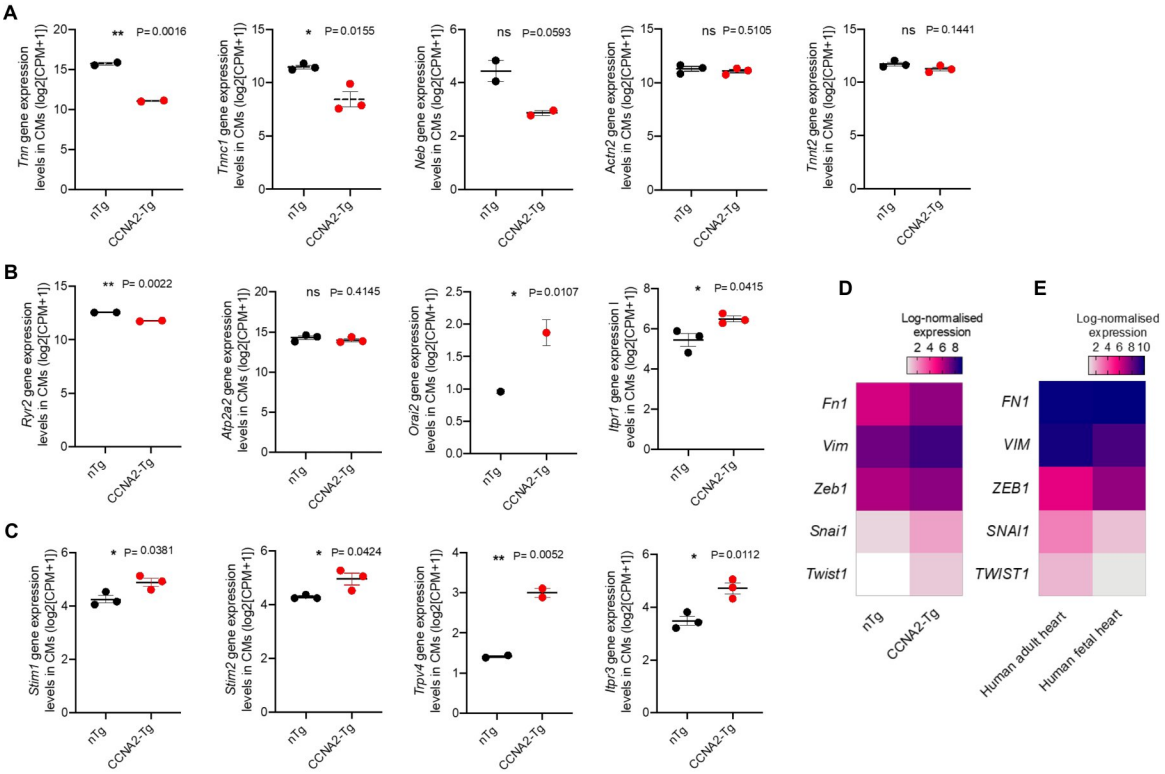

Figure S1. A) Representative scatter plots of sarcomere assembly genes *(Neb, Tnn, Tnnc1, Actn2,* and *Tnnt2),* and **B)** Ca^{2+} handling genes (*Ryr2, Atp2a2, Slc8a1*, and others) in nTg and CCNA2-Tg cardiomyocytes as delineated from bulk RNA seq. Each point represents an individual value; the mean value is represented by the horizontal line. Error bars represent SEM, with statistical significance indicated (*P*-values). ns denotes non-significant differences. **C)** Heatmap of log-normalized expression of mesenchymal transition markers (*Fn1, Vim, Zeb1, Snai1, and Twist1*) in nTg and CCNA2-Tg cardiomyocytes, as well as **D)** human adult and fetal hearts. Gene expression levels are log-transformed and normalized.

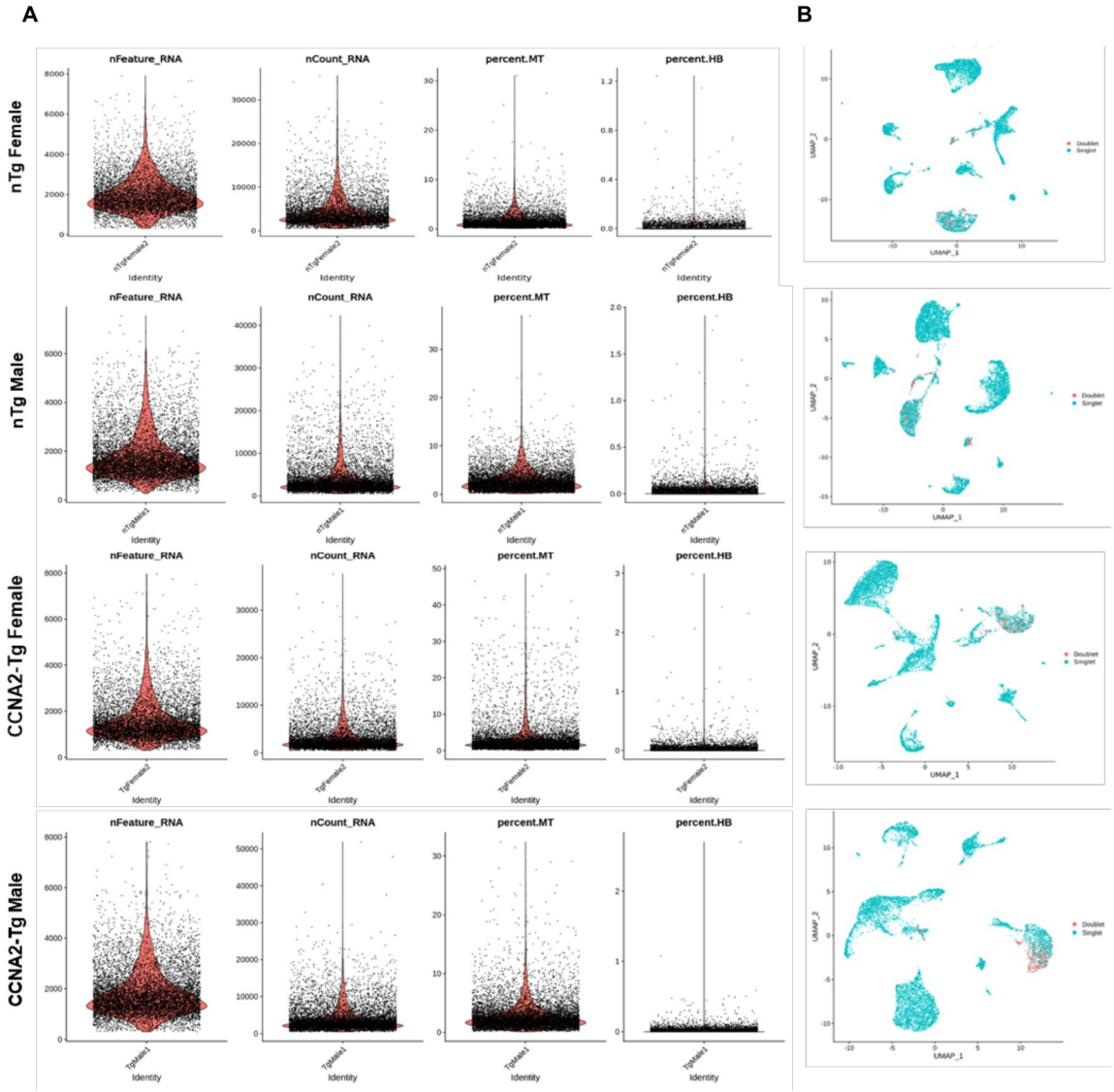

Figure S2. Quality control (QC) filtering and visualization in SnRNA-seq. A) "nFeature_RNA" indicates the count of gene features; "nCount_RNA" represents the count of UMIs; "percent.MT" signifies the proportion of counts originating from mitochondrial genes, and "percent.HB" signifies the proportion of counts stemming from Hemoglobin-related genes in all conditions nTg and CCNA2-Tg males and females. Each data point corresponds to a cell. **B)** The UMAP plots are generated from the top principal components within the clustered dataset. Each data point represents an individual cell and is color-coded based on whether it is categorized as a singlet or doublet.

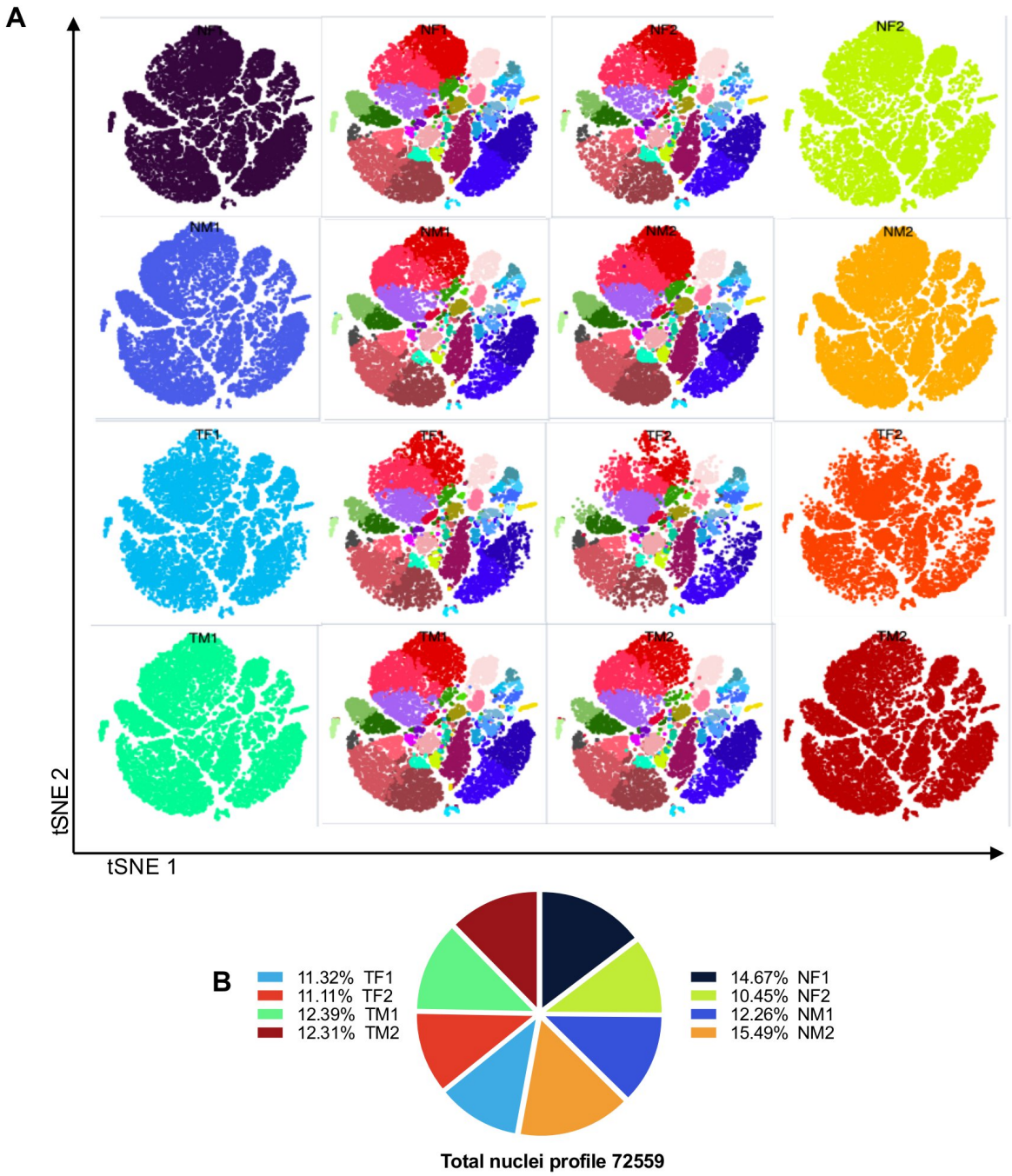

Figure S3. A) t-SNE plot clustering the nuclei of nTg and CCNA2-Tg conditions (*n*=8 total). **B)** Pie chart representing the percentage of nuclei profile in all conditions of nTg and CCNA2-Tg mice. (*n*= 72,559 total nuclei)

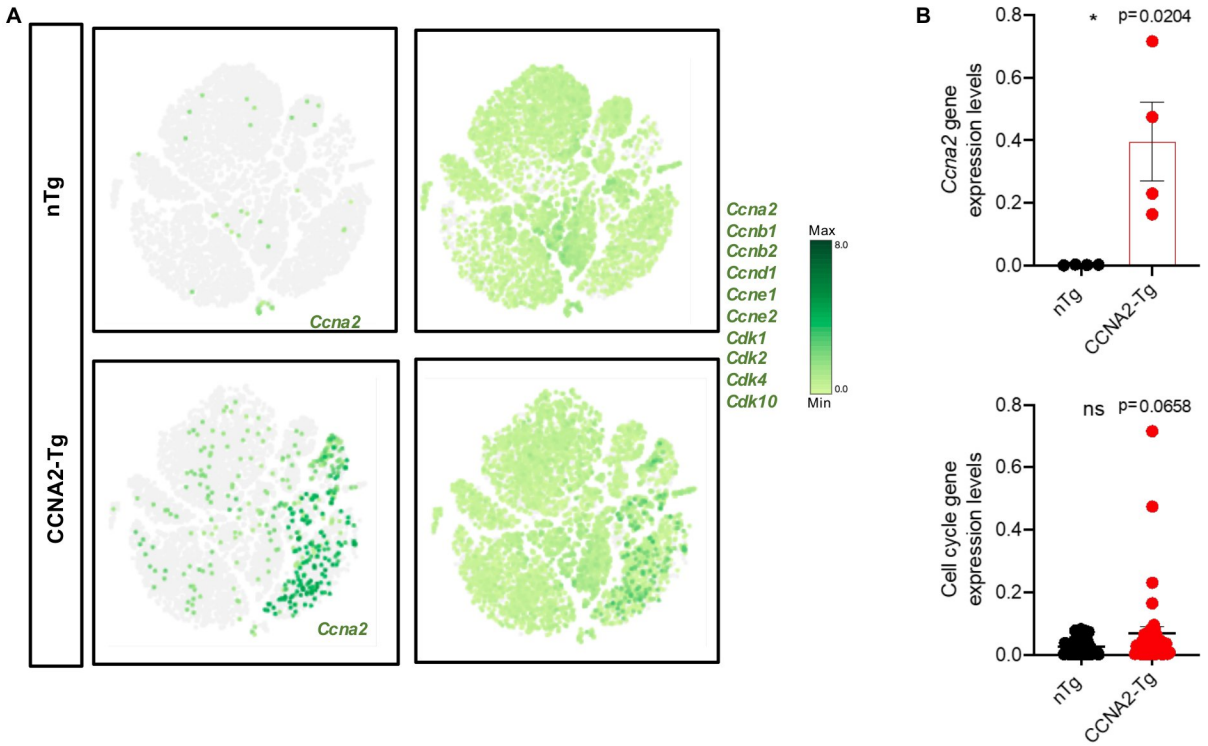

964
965 **Figure S4. A)** t-SNE plots and **B)** representative scatter plots of CCNA2 and cell cycle genes
966 expression across the combined transcriptomic profiles of all subclusters of nTg and CCNA2-Tg
967 mice. Bars represent mean ± s.e.m. Each point represents an individual value; the mean value is
968 represented by the horizontal line. Error bars represent s.e.m.

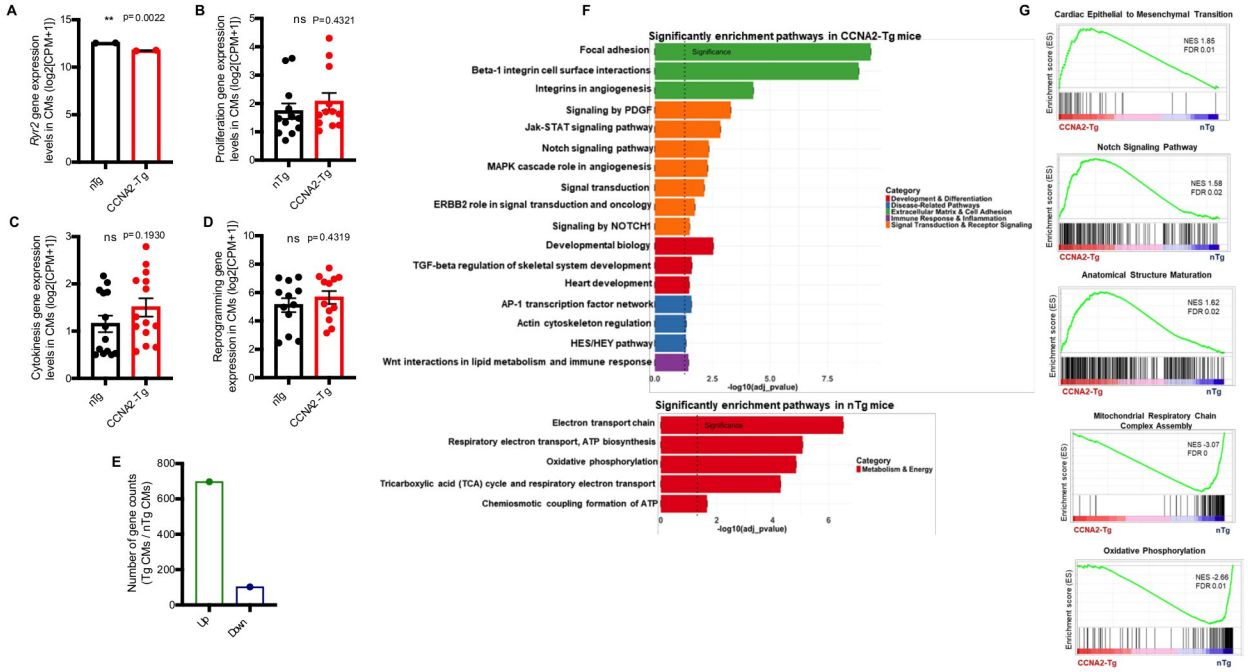

Figure S5. A) Representative scatter plots of cardiomyocyte maturation gene *Ryr2, **B)*** proliferation, **C)** cytokinesis, and **D)** reprogramming gene expression in nTg and CCNA2-Tg cardiomyocytes. Each dot represents an individual value, and bars indicate mean ± s.e.m. **E)** Number of differentially expressed genes (Up or Down) in adult CCNA2-Tg mouse cardiomyocytes as compared to adult nTg mouse cardiomyocytes. **F)** Significantly enriched pathways in adult CCNA2-Tg and nTg mouse cardiomyocytes (P-value adjusted <0.05), analyzed using BioPlanet. **G)** Gene set enrichment analysis (GSEA) in CCNA2-transgenic versus nTg cardiomyocytesshowing a significant downregulation of oxidative phosphorylation and mitochondrial respiratory chain complex assembly pathways in CCNA2-transgenic cardiomyocytes, may suggest a metabolic shift consistent with dedifferentiation. Conversely, pathways such as cardiac epithelial-to-mesenchymal transition (EMT) and Notch signaling were upregulated, indicating activation of developmental and reprogramming pathways that facilitate a more regenerative state.

Movie S1. The real-time, live-imaging movie of human adult cardiomyocytes (55-year-old male) as described in **Figure 1.**

Movie S2. Real-time, live-imaging movie of human adult cardiomyocytes (41-year-old female) as described in **Figure 1.**